The Influence of HCl on the Evaporation Rates of H_2O over Water Ice in the Range 188 to 210 K at small Average Concentrations

Christophe Delval[1,2,a] and Michel J. Rossi[1,3]

[1]Laboratory of Air and Soil Pollution Studies (LPAS), ENAC Faculty, Swiss Federal Institute of Technology (EPFL), CH-1015 Lausanne, Switzerland

[2]Atmospheric Particle Research Laboratory (APRL), ENAC Faculty, Swiss Federal Institute of Technology (EPFL), CH-1015 Lausanne, Switzerland

[3]Laboratory of Atmospheric Chemistry (LAC), Paul Scherrer Institute (PSI), CH-5232 Villigen-PSI, Switzerland

[a]Present Address: Patent Examiner - Directorate 1657, Dir. 1.6.5.7, European Patent Office, Patentlaan 3-9, 2288 EE Rijswijk, Netherlands

Corresponding author: michel.rossi@psi.ch

ABSTRACT

The evaporation flux $J_{ev}(H_2O)$ of H_2O from HCl-doped typically 1.5 μm or so thick vapor-deposited ice films has been measured in a combined quartz crystal microbalance (QCMB) – residual gas mass spectrometry (MS) experiment. $J_{ev}(H_2O)$ has been found to show complex behaviour and to be a function of the average mole fraction χ_{HCl} of HCl in the ice film ranging from $6x10^{14}$ to $3x10^{17}$ molecule cm^{-2} s^{-1} at 174 – 210 K for initial values χ^0_{HCl} ranging from $5x10^{-5}$ to $3x10^{-3}$ at the start of the evaporation. The dose of HCl on ice was in the range of 1 to 40 formal monolayers and the H_2O vapor pressure was independent of χ_{HCl} within the measured range and equal to that of pure ice down to 80 nm thickness. The dependence of $J_{ev}(H_2O)$ with increasing average χ_{HCl} was correlated with (a) the evaporation range $r^{b/e}$ parameter, that is the ratio of $J_{ev}(H_2O)$ just before HCl-doping of the pure ice film and $J_{ev}(H_2O)$ after observable HCl desorption towards the end of film evaporation, and (b) the remaining thickness d_D below which $J_{ev}(H_2O)$ decreases to less than 85% of pure ice. The dependence of $J_{ev}(H_2O)$ with increasing average χ_{HCl} from HCl-doped ice films suggests two limiting data sets, one associated with the occurrence of a two-phase pure ice/crystalline HCl hydrate binary phase (set A), and the other with a single phase amorphous HCl/H_2O binary mixture (set B). The measured values of $J_{ev}(H_2O)$ may lead to significant evaporative life-time extensions of HCl-contaminated ice cloud particles under atmospheric conditions, regardless of whether the structure corresponds to an amorphous or crystalline state of the HCl/H_2O aggregate.

1. **INTRODUCTION**

HCl is among the mineral acids that control the acidity of the atmosphere together with HNO_3 and H_2SO_4. The production of atmospheric HCl is predominantly taking place in the middle and upper stratosphere where O_3 is formed owing to photolysis of halogen containing source gases such as CFC's (chlorofluorocarbons). However, there are no known sources of HCl in the upper troposphere (UT) because scavenging processes of HCl throughout the troposphere are very efficient which leads to HCl background concentrations of less than 0.1 ppb (Graedel and Keene, 1995). The absence of significant sources in the troposphere, the long photolytic lifetime of HCl and the fact that the production region is well separated from the regions of interest, namely the UT and the lower stratosphere (LS) all contribute to the fact that HCl is an excellent tracer for stratospheric ozone in the UT (Marcy et al., 2004). Owing to the frequent occurrence of Cirrus clouds in this atmospheric region it is of obvious interest to study the interaction of HCl with atmospheric ice particles at relevant temperature and pressure conditions (Jensen et al. 2001; Zerefos et al., 2003). The compact correlation between O_3 and HCl has been used to monitor stratospheric-tropospheric exchange processes and stratospheric O_3 intrusions into the troposphere that are still an active field of investigation (Houghton et al, 2001).

HCl is of importance in the LS as it partakes in heterogeneous reactions on Polar Stratospheric Ice Clouds (PSC's) as well as on background stratospheric H_2SO_4 aerosol according to the following reaction taken as an example:

$$HCl(ads) + ClONO_2 \rightarrow Cl_2(g) + HNO_3(ads)$$

These reactions efficiently convert inactive Cl-containing reservoir molecules such as HCl and $ClONO_2$ into active photolyzable Cl-containing compounds in a single reaction. Typical examples of such photolabile reaction products are Cl_2, $ClNO_2$ and HOCl that will change the atmospheric composition owing to the high reactivity of the photolysis products such as atomic Cl (Solomon et al., 1986; Tolbert et al., 1987; WMO 2003). It thus follows that HCl is of stratospheric importance and is frequently used as a model compound for heterogeneous reactions on ices that has inspired many laboratory kinetic studies (Leu et al., 1991; Hanson and Ravishankara, 1992; Chu et al., 1993; Flückiger et al., 1998; Hynes et al., 2001; Abbatt, 2003).

HCl forms hydrates of variable stoichiometry when exposed to ice depending on the temperature of deposition and the partial pressure of HCl (Ortega et al., 2004; Graham and Roberts, 1997). X-Ray diffraction has allowed the identification of four crystalline hydrates

containing one (Yoon and Carpenter, 1959), two (Lundgren and Olovson, 1967), three (Lundgren and Olovson, 1967a) and six (Taesler and Lundgren, 1978) H_2O per HCl molecule. In addition, amorphous mono-, tetra- and hexahydrates have been reported under various experimental conditions (Yoon and Carpenter, 1959; Delzeit et al., 1993). The control of growth conditions of a specific HCl hydrate is sometimes elusive, but the formation of a saturated HCl hexahydrate phase has been reported at sufficiently large HCl exposure (Graham and Roberts, 1995) using amorphous ice as a starting point despite the fact that the hexahydrate is said to nucleate with difficulty, at least in thin films (Ortega et al., 2004). However, the molecular and dynamic details of the crystallization process have not been investigated as yet.

Fourier-Transform IR (FTIR) absorption measurements have enabled the characterization of both amorphous as well as crystalline HCl hydrates at growth conditions that are sometimes significantly different compared to the samples investigated using X-Ray diffraction. Vibrational spectra of HCl hydrates in the mid IR have been routinely used for identification purposes for some time (Ferriso and Hornig, 1955; Gilbert and Sheppard, 1973). Recently, the mid IR absorption spectra of the four HCl hydrates mentioned above have been assigned in a comprehensive and definitive way, albeit without simultaneous proof of the crystalline structure using X-Ray diffraction (Buch et al., 2002; Xueref and Dominé, 2003). More recently, the reflection absorption IR spectrum (RAIR) of crystalline HCl hexahydrate in the mid-IR range has been recorded and assigned using theoretical calculations based on density functional theory that results in a refinement of the geometric structure of the HCl hydrates and a prediction of the vibrational modes of the crystal (Ortega et al., 2004). It must be recalled that FTIR spectra in transmission and reflection may in most cases not be directly compared across the mid IR range.

Regarding the nature of the HCl-ice adsorbate one of the important questions is whether adsorbed HCl is ionized or exists as a molecular adsorbate under atmospherically relevant conditions of the UT/LS. This will determine the mechanism of the heterogeneous reaction which constitutes necessary knowledge for the extrapolation of heterogeneous reaction rates measured in the laboratory to atmospheric conditions. Thermal desorption of HCl monitored by IR absorption in the mid-IR range revealed a molecularly adsorbed state of HCl desorbing below 50 K (Delzeit et al., 1993a). IR studies performed by Banham et al. on HCl-ice films failed to detect molecularly adsorbed HCl at $T \geq 90$ K despite the high rate of HCl adsorption in that temperature range (Banham et al., 1995). In contrast, Graham and Roberts attributed a characteristic Temperature Programmed Desorption (TPD) peak of a

HCl/amorphous ice adsorbate monitored by residual gas MS and occurring at 150 K to molecularly adsorbed HCl (Graham and Roberts, 1995). However, they did not report the IR absorption spectrum of the adsorbate in the mid-IR nor did they explain why molecular adsorption of HCl exclusively occurred on amorphous, but not on crystalline ice. Most recent results seem to point towards the existence of molecularly adsorbed HCl on ice below 50 K and at submonolayer coverages in coexistence with ionized solvated HCl whose fraction increases with increasing ice temperature (Buch et al., 2002; Delzeit et al, 1993a; Delzeit et al. 1997; Uras et al., 1998; Devlin et al., 2002; Lu and Sanche, 2001). Kang et al. discovered that both molecularly adsorbed as well as ionized HCl coexisted on ice that was deposited under Ultra-High Vacuum (UHV) conditions in the temperature range 50 to 140 K and under conditions of low HCl exposure (Kang et al., 2000).

Although theoretical electronic structure calculations predict spontaneous ionization of adsorbed HCl (Gertner and Hynes, 1996; Bolton and Petterson, 2001) most experiments point towards a seemingly thermally activated ionization process that may be enabled by structural factors of the ice matrix that are themselves a function of temperature. Consistent with these results concentration profiling experiments of HCl/ice adsorbates using static Secondary Ionization Mass Spectroscopy (SIMS) techniques failed to discover molecularly adsorbed HCl on ice in the range 90-150 K (Donsig and Vickerman, 1997). In conclusion, both experimental and theoretical studies clearly point to the absence of significant quantities of molecularly or covalently adsorbed HCl under stratospheric conditions. Instead, HCl is ionized and solvated by H_2O on the surface of ice films and may occur either as amorphous HCl/H_2O hydrates of undefined stoichiometry or as crystalline HCl hydrates. However, these facts do not rule out the presence of small amounts of molecularly adsorbed HCl on ice that may be intermediates in the complex mechanism of HCl adsorption on ice as evidenced by the negative temperature dependence of the rate of uptake of HCl on ice (Flückiger et al., 1998). In fact, such an intermediate has been invoked in the description of HCl adsorption on ice under atmospheric conditions using a chemical kinetic model based on a multitude of experimental observables collected upon HCl uptake on ice (Flückiger and Rossi, 2003).

Work by Parent and coworkers uses Near-Edge X-Ray Absorption Spectroscopy (NEXAFS) of HCl-doped low temperature ice substrates in order to determine the relative population of ionic and covalently bound HCl and distinguish between bulk and HCl surface states in the temperature range 20 to 150 K (Bournel et al., 2002; Parent and Laffon, 2005). The results seem to confirm the consensus on the low-temperature existence of molecularly adsorbed HCl up to 90 K beyond which an increasing amount of HCl is converted into an

ionic form, such as $H_3O^+Cl^-$ (Eigen cation) or $H_5O_2^+Cl^-$ (Zundel cation) formed by spontaneous ionization of adsorbed HCl on ice, up to completion at 150 K (). The newest work by Parent compares NEXAFS with photoemission (UPS, XPS) and FTIR in transmission of thin HCl/H_2O films (Parent et al., 2011). The results are roughly consistent but surprising in the sense that these workers find 92% ionically dissolved HCl in/on ice at 50 K in contrast to Kang et al. (2000) and Devlin et al. (2000) under similar exposure (dose) and temperature conditions. In addition, Parent et al. (2011) perform the NEXAFS experiment on a (thick) 100 ML "crystalline" H_2O ice substrate deposited at 150 K whereas the photoemission and FTIR absorption experiments used a 4 ML thin ice slab deposited at 120 K. The question has to be raised whether the two types of used ice films may be responsible for some of the discrepancies in the results because both the density and the structure of ice are known to be a strong function of temperature and deposition conditions (Kuhs et al., 2012; Schriver-Mazzuoli et al., 2000). The most recent work of Parent et al. (2011) sparked an interesting controversy in the assignment of the FTIR absorption spectrum of thin HCl/H_2O films and led to two comments showcasing the difficulties of intercomparison of nominally identical experiments (Devlin and Kang, 2012; Parent et al., 2012).

Furthermore, the results indicate that the "dangling bonds" of the ice surface attributed to isolated OH groups are not the unique site of HCl adsorption, even in the range 20-90 K (Flückiger and Delval, 2002). The present work suggests that maiden uptake of HCl onto pure ice weakens and perturbs the crystal structure of the ice matrix in an irreversible way such that additional sites for HCl adsorption and ionization are created akin to Parent et al. (2011). Initial HCl uptake on pure ice therefore has a catalytic effect on the following HCl uptake. This irreversible nature of initial HCl dosing is known for several years and has been observed some time ago in Knudsen flow reactor studies on the HCl/H_2O system under steady-state conditions of both HCl and H_2O at temperatures representative of the UT/LS (Flückiger et al., 1998; Oppliger et al., 1997). The most recent experimental work on HCl/H_2O at an atmospherically relevant ("warm") temperature (253 K) has examined the HCl depth profile using XPS spectroscopy and finds molecularly adsorbed (physisorbed) HCl at its outermost layer and ionic dissociation in deeper layers (Kong et al., 2017). Complementary X-Ray absorption results also point towards a perturbation of the crystal structure of ice in the aftermath of HCl adsorption/dissolution into deeper layers of ice.

We have concluded from recent work that HCl doping in quantities of submonolayer to several monolayers of HCl leads to the decrease of both the evaporative flux J_{ev} (molecule $cm^{-2}s^{-1}$) or rate R_{ev} (molecule $cm^{-3}s^{-1}$) and the rate of condensation k_{cond} (s^{-1}), of H_2O in the

presence of ice without perturbing the equilibrium vapour pressure of H_2O, P_{H2O}^{eq} (Delval et al., 2003). We have furthermore shown that the way J_{ev} of H_2O decreases with time depends on the rate of deposition or the integral of deposited HCl, namely R_{HCl} (molecule s^{-1}) and N_{HCl} (molecule), respectively. It appears that two observed HCl species on/in ice, namely single phase amorphous HCl/H_2O mixtures and a binary phase consisting of pure ice and an as yet unidentified crystalline HCl hydrate, HCl•xH_2O, decrease $J_{ev}(H_2O)$ to a different extent as proposed in Delval et al. (2003). These results have led us to perform systematic experiments in this work using the Quartz Crystal MicroBalance (QCMB) combined with residual gas Mass Spectrometry (MS) that we have used successfully in the past (Delval and Rossi, 2004) in order to investigate the temporal change of $J_{ev}(H_2O)$ with the increasing average mole fraction of HCl, χ_{HCl}, remaining in the ice. One of the goals of the present work is to determine the influence of the HCl deposition parameters on the temporal change of J_{ev} and the mass accommodation coefficient α during evaporation of a HCl-doped ice film and its consequence on the lifetime of atmospheric ice particles contaminated by HCl. This issue is key in relation to the importance of heterogeneous vs. homogeneous atmospheric reactions at midlatitudes as has been pointed out in the past (Solomon et al., 1986; 1997).

2. EXPERIMENTAL

The emphasis of the present experiments was placed on the deposition of small amounts of HCl ranging in doses from 1 to 40 formal monolayers of HCl where a formal monolayer of adsorbed HCl corresponded to a surface concentration of 2.5×10^{14} molecule cm^{-2} (Table A1) which is a consensus value obtained from several selected experiments. The apparatus as well as the methods used for calibration and the HCl deposition procedure have been described in detail elsewhere (Delval and Rossi, 2005). The experimental conditions are generally identical to the ones presented in Delval and Rossi (2005) and the instrumental parameters are summarized in Table 1. The only significant difference between the study of HNO_3-doped ice and the present condensed phase investigation of HCl-doped ice lies in the mode of trace gas admission. HCl was deposited by backfilling the reactor under stirred flow conditions with the inlet tubing used for trace gas injection oriented towards one side of the Si-window of the cryostat set at ambient temperature whereas HNO_3 was deposited by directed injection onto ice films supported by the quartz crystal of the QCMB as referenced above. Evaporation experiments have been performed isothermally on samples in the

temperature range 174-210 K under dynamic pumping conditions, that is at maximum pumping speed (gate valve open) in order to prevent readsorption of HCl on the ice substrate.

First, an approximately 1.5 μm thick ice film was grown at 190 K on the quartz crystal of the QCMB by deposition of bidistilled water vapor at a rate of $1x10^{17}$ molecule cm^{-2} s^{-1} under static conditions. The H_2O equilibrium vapor pressure agreed with published values across the covered temperature range (Marti and Mauersberger, 1993; Mauersberger and Krankowsky, 2003). Subsequently, the system was set to the desired temperature given in Table 2 (second column from the left) and a metered amount of HCl was deposited under stirred flow conditions. The rate of deposition of HCl, R_{HCl}, as well as its time integral, namely the number of HCl molecules deposited on ice, N_{HCl}, have been evaluated using the method described in Delval and Rossi (2005). Typically, R_{HCl} ranges between $8.0x10^{11}$ and $4.2x10^{13}$ molecule s^{-1} and N_{HCl} between $1.0x10^{14}$ and $5.4x10^{15}$ molecules. The experimental conditions of HCl-deposition as well as important experimental parameters are reported in Table 2. Finally, the system was set to dynamic pumping conditions by opening the gate valve to the turbopump. $J_{ev}(H_2O)$ was measured isothermally using both the QCBM and residual gas MS. Figure 1 illustrates a typical experimental protocol of the evaporation at 192 K of a HCl-doped ice film labelled as experiment 11 in Table 2 and performed as a multidiagnostic experiment where both the gas- as well as the condensed phases are simultaneously monitored.

At t = 0, the system is set from stirred flow to dynamic pumping that starts the evaporation experiment. The continuous curve marked with the empty squares symbol in Figure 1A corresponds to J^{QCM}_{ev}, the evaporative flux of H_2O calculated from the raw signal at the output of the QCMB. The diamond symbol (◊) corresponds to J^{18}_{ev} evaluated from I^{18}, the MS signal amplitude for H_2O monitored at m/e = 18. Int(J^{18}_{ev}) marked by triangles in Figure 1A is the time integral of J^{18}_{ev} and corresponds to the total number of H_2O molecules that have evaporated from the ice film at t. D is the label at time t_D at which $J_{ev}(H_2O)$ decreased from its original value corresponding to pure ice to 85% of its original value at t = 0, and d_D is the remaining thickness of the ice film at t_D. H_b and H_e in Figure 1B correspond to the time when HCl evaporation begins and ceases to be observed, respectively, using gas phase residual mass spectrometry (x symbols in Figure 1B) and are labeled t_{Hb} and t_{He}. The data have been treated in analogy to HNO_3-doped ice through the formalism given in Delval and Rossi (2005). Akin to HNO_3 the mass balance between HCl deposited, N^{dep}_{HCl}, and HCl recovered during ice evaporation, N^{evap}_{HCl}, agrees to within less than a factor of 2 under dynamic pumping conditions. We therefore estimate the average uncertainty (2σ) of the HCl

mole fraction χ_{HCl} of ± 18 % from the average discrepancy between N^{dep}_{HCl} and N^{evap}_{HCl} displayed in Table 2. In the following N_{HCl} will always refer to N^{dep}_{HCl} derived from the measurement of HCl at deposition because it refers to a directly measured quantity originating from a measured pressure decrease in a given volume and time interval $\Delta P/\Delta t$. The present experiments cover the evaporation of a small albeit important fraction of the model ice film for which the decrease of $J_{ev}(H_2O)$ is significant.

3. RESULTS

The experimental data reported in Table 2 on the isothermal change of the evaporative flux of water, $J_{ev}(H_2O)$, as a function of the average mole fraction of HCl, χ_{HCl}, in the remaining ice film during the evaporation process under dynamic conditions are presented in Figure 2. Dynamic pumping conditions ensure the absence of any readsorption of H_2O vapor during evaporation owing to the low H_2O partial pressures in the reactor. The axes labelled "b" and "e" correspond to the values of $J_{ev}(H_2O)$ at the end of ice film deposition and after desorption of most of the adsorbed HCl from the HCl-doped ice film at t_{He}, respectively, as displayed in Figure 1B. The average mole fraction χ_{HCl} of HCl in the remaining ice film as a function of time is calculated according to Delval and Rossi (2005). The change in χ_{HCl} owing to H_2O evaporation is evaluated between $t = t_D$ and $t = t_{Hb}$ that corresponds to the time interval when the number of adsorbed HCl molecules is constant as no release of HCl is observable in the gas phase at m/e = 36 before t_{Hb}. Table 2 also displays the initial value of the HCl mole fraction, χ^0_{HCl}, calculated for the ice film just at the end of HCl deposition and marked by a colored circle on the experimental trajectory of a color-coded evaporating ice film displayed in Figure 2. The average mole fraction of HCl in the ice film, χ_{HCl}, increases owing to evaporation of H_2O from the ice film without loss of HCl such that the elapsed time increases with χ_{HCl} in Figure 2.

The beginning of an evaporation experiment after the end of HCl doping (t = 0 in Figure 1 or t_0 in Figure 2) is marked by a colored circle of a given experiment whose parameters are displayed in Table 2 and Figure 2 (see experiment 8). As pointed out above, at $t = t_D$ $J_{ev}(H_2O)$ has decreased to an arbitrarily chosen value of 85% of its original value measured at $t = t_0$ that corresponds to the beginning of the bold color-coded smooth curve of a given experiment. Figure 2 essentially displays trajectories of evaporation experiments from t_0 (colored circle) moving to t_D and finishing at t_{Hb} between the two limiting values for pure ice

(color coded number of a given experiment on axis "b" for "beginning") and the remaining ice film at the end of measurable HCl desorption t_{He} (color-coded number of experiment on axis "e" for "Halogen end"). The trajectory of an experiment with values of χ_{HCl} between t_0 (colored circle at χ^0_{HCl}) and t_D (beginning of bold colored line, see experiment 8 in Figure 2) ending at t_{Hb} (end of bold line, experiment 8) is presented as a bold dashed-dotted and bold smooth line from t_0 to t_{Hb}, respectively, in order to emphasize the quantitative portion of the experiment. Thinner (color-coded) dotted lines connect the end of ice film deposition (colored circle on axis "b") and HCl-dosing with t_0, the beginning of the evaporation experiment and also describe the post-phase of evaporation starting at t_{Hb} to t_{He} in order to guide the eye of the reader to imagine a complete evaporation cycle.

Two different data sets of the change of $J_{ev}(H_2O)$ with χ_{HCl} may be distinguished in Figure 2. The first kind of data set corresponds to the curves describing J_{ev} for experiments 1, 2, 9 and 11 and is called dataset A. These traces present a slow continuous decrease of $J_{ev}(H_2O)$ as χ_{HCl} increases during H_2O evaporation. The second type of dataset shows an initial plateau of $J_{ev}(H_2O)$ with increasing χ_{HCl} starting at the value of pure ice evaporation followed by a sudden decrease of $J_{ev}(H_2O)$ and is found for experiments 3, 4, 7 and 8 which we call dataset B. Akin to HNO_3, we have evaluated the impact of the HCl deposition protocol on the evaporation range parameter, $r^{b/e}$, which is the ratio between the evaporative flux of H_2O at the beginning of ice evaporation, $J^b_{ev}(H_2O)$ reported on the left axis "b" in Figure 2, and $J_{ev}(H_2O)$ close to the end of the desorption of HCl, $J^e_{ev}(H_2O)$, at $t = t_{He}$ (the right axis "e" in Figure 2). It describes the factor by which $J_{ev}(H_2O)$ decreases within the limits of "b" and "e". The impact of both the rate of deposition of HCl on ice, R_{HCl}, and its time integral corresponding to the dose of deposited HCl, N_{HCl}, are presented in Figures 3 and Figure A1 (Appendix), respectively.

It appears from these Figures that we have not succeeded to find a simple experimental parameter that controls $J_{ev}(H_2O)$ either with elapsed time or amount of adsorbed HCl expressed as the time dependence of χ_{HCl}. Instead, the data may roughly be classified along the two cases presented above, namely datasets A and B. The distinction between both data sets seems to be the rate of change (slope) of $J_{ev}(H_2O)$ within a fairly narrow range of χ_{HCl}. Indeed, the available number of experiments clearly shows two distinct and limiting cases whereas the search for other controlling parameters such as R_{HCl}, N_{HCl} and the temperature of deposition (T_{ice}) for dataset A failed akin to a similar HNO_3 study (Delval and Rossi, 2005).

One may take note for instance of the low value of χ_{HCl} at 210 K for experiment 9 where the conditions of deposition are similar to experiments 1 and 2, yet, its respective

values of $r^{b/e}$ differ significantly from experiment 9 (Figure 3). In contrast, for dataset B the $r^{b/e}$ values are similar for the whole set and range from 20 to 27.2 staying within a fairly narrow band. Moreover, they seem to be independent of R_{HCl} and N_{HCl} as for data set A. In contrast, the $r^{b/e}$ values for dataset A seem widely scattered over the explored parameter space. We have also investigated the impact of the deposition protocol on d_D, which is the thickness of ice that is affected by the presence of HCl, namely the remaining thickness of ice whose $J_{ev}(H_2O)$ value has decreased to 85% of $J_{ev}(H_2O)$ of pure ice. The results on d_D as a function of R_{HCl} and N^{dep}_{HCl} are presented in Figures 4 and A2 (Appendix), respectively. Taking the results of Figures 3, 4, A1 and A2 together we arrive at the following two conclusions:
(1) T_{ice}, R_{HCl} and N^{dep}_{HCl} are not controlling parameters or predictors for $J_{ev}(H_2O)$ of either set.
(2) The evaporation range parameters $r^{b/e}$ and d_D are not characterizing set A. In contrast, for dataset B, $r^{b/e}$ and d_D values fall into a narrow range with values varying from 460.7 to 636.0 nm compared to the original ice thickness d_0 of 1'500 nm or so (exact numbers in Table 2).

4. DISCUSSION

Figure 1 displays the evaporation history of sample 11 as an example whose deposition parameters are listed in Table 1. The initial average mole fraction χ_{HCl}^0 of HCl, once deposition on the 1.44 μm thick ice film under stirred flow reactor conditions is terminated, has been estimated from the total number of H_2O molecules contained in the ice film and the measured number of deposited HCl molecules, N^{dep}_{HCl}, for experiment 11 (Table 2). Table 2 and Figure 1 reveal that for approximately 2.2×10^{18} H_2O molecules in the film and 5.4×10^{14} molecules of deposited HCl, we obtain $\chi_{HCl}^0 = 2.7 \times 10^{-4}$. This HCl mole fraction represents an average value that takes into account all H_2O molecules contained in the ice film whereas in reality there will be a HCl gradient across the ice film as has been observed in the case of the HNO_3/ice system (Delval and Rossi, 2005).

After the HCl deposition process on the typically 1.5 μm thick ice film the gate valve is opened in order to initiate the isothermal evaporation experiment under dynamic pumping conditions. Initially, H_2O evaporates at fluxes $J_{ev}(H_2O)$ that are characteristic of pure ice measured previously (Delval and Rossi, 2004; Pratte et al., 2006). These initial values $J_{ev}^b(H_2O)$ are displayed on the left-hand "b" (= "beginning") axis in Figure 2. As the evaporation proceeds $J_{ev}(H_2O)$ slightly decreases with time as displayed in Figure 1A to the arbitrarily chosen point where $J_{ev}(H_2O)$ has decreased to 85% of the initial pure ice value at which point the remaining ice thickness d_D has decreased by approximately one third to 771.7

nm remaining ice thickness as displayed in Figure 1B and Table 2. Further evaporation of H_2O leads to a continuous decrease of $J_{ev}(H_2O)$ at a corresponding increase of χ_{HCl} up to point H_b defined above ("Halogen beginning") at t_{Hb} (Figure 1B) where HCl starts to desorb from the ice film as monitored using the residual MS signal at m/e = 36.

For $t < t_{Hb}$, χ_{HCl} is given by the number of originally deposited HCl molecules that remain adsorbed on the ice film up to t_{Hb} and the remaining H_2O molecules in the film. In contrast, for $t > t_{Hb}$ the composition of the remaining ice film must be determined by taking into account the loss by evaporation of both H_2O and HCl. The present experimental configuration is not adapted to quantitatively measure HCl loss. Therefore, we have chosen to display the temporal development of $J_{ev}(H_2O)$ for $t < t_{Hb}$ in Figure 2 as a function of the average value of the HCl mole fraction χ_{HCl}. However, the value of $J_{ev}(H_2O)$ at $t = t_{He}$ where most of the HCl has desorbed from the ice film is plotted on the right axis labelled "e" (= "end") as $J_{ev}^{e}(H_2O)$ in Figure 2 in order to provide a limit for the minimum value of the evaporation rate $J_{ev}(H_2O)$ at an ice film thickness d_{He} of approximately 80 ± 10 nm as displayed in Figure 1B. We have observed in the past that $J_{ev}(H_2O)$ for a pure ice film of approximate thickness of 80 nm or less also slows down, presumably owing to island formation at the very end of pure thin ice film evaporation (Delval and Rossi, 2005). Therefore, results are becoming more difficult to interpret such that we halted the experiment at t_{He}. The ratio $r^{b/e} = J_{ev}^{b}(H_2O)/J_{ev}^{e}(H_2O)$ is displayed in Table 2 and is an operational evaporation range parameter that estimates the extent of decrease of $J_{ev}(H_2O)$ for a thick HCl-doped ice film of μm size down to thicknesses of approximately 80 nm.

At the start of the evaporation experiment the equilibrium vapor pressure of H_2O, $P_{eq}(H_2O)$, is that of pure ice (Delval et al., 2003; Delval and Rossi, 2004; Pratte et al., 2006) owing to the small values of χ_{HCl}^{0}. Raoult's Law applies to such small values of χ_{HCl} but leads to unmeasurably small deviations from the observed vapor pressure of H_2O which is that of pure ice. In fact, we have never observed an equilibrium vapor pressure that did not correspond to pure ice in the course of the present work that seems to be the consequence of the small average mole fractions of HCl in the H_2O/HCl system. This value of $P_{eq}(H_2O)$ is observed throughout the evaporation up to t_{He} as the film is apparently sufficiently H_2O-rich to support an equilibrium vapour pressure characteristic of pure ice consistent with the published, albeit revised HCl/H_2O phase diagram by Iannarelli and Rossi (2014). In view of the decreasing values of $J_{ev}(H_2O)$ displayed in Figure 2 the equilibrium vapour pressure of pure ice can only be maintained if the condensation rate coefficient k_c for H_2O adsorption decreases to the same extent as $J_{ev}(H_2O)$ in agreement with previous work (Delval et al.,

2003; Delval and Rossi, 2004; Pratte et al., 2006) and the concept of microscopic reversibility.

Figure 1A displays both the QCMB signal (□) as well as the corresponding MS signal for evaporating H_2O at m/e = 18 (◊). Akin to the HNO_3/H_2O system studied previously (Delval and Rossi, 2005) we obtain a perfect match between the two signals for $t < t_D$ whereas for $t > t_D$ there is a significant discrepancy, especially at t > 300 s amounting to typically less than a factor of two. Such a disagreement has been noted before for HNO_3/H_2O, albeit to a larger extent. The reason for this behaviour of the QCMB signal has not been studied in detail but may well lie in a structural rearrangement of the condensed phase during evaporation that will lead to a change in the calibration factor C_f defined in Table 1 and in Delval and Rossi (2005). In view of the straightforward interpretation of the calibrated MS signal at m/e = 18 we have used it for the measurement of $J_{ev}(H_2O)$ at $t > t_D$ akin to the previous study on HNO_3/H_2O.

The accuracy with which both t_{Hb} and t_{He} can be determined depends on the temporal change of the background MS signal for HCl at m/e = 36 displayed in Figure 1B following the dosing of the thin ice film under stirred flow conditions. Figure 1B displays the MS signal at m/e = 36 as a function of time just before the start of HCl desorption at t_{Hb} that is signalled by an increase in the MS intensity whereas t_{He} corresponds to the return of the HCl signal to the decaying HCl background in comparison to a reference experiment in which the HCl background was monitored as a function of time following the admission of the same HCl dose in the absence of an ice film. We estimate that t_{Hb} is determined to ± 10 s whereas t_{He} may only be estimated to ± 100 s by virtue of the vanishing intensity of the HCl MS signal compared to its slowly decaying background.

Previous work has established that the rate of deposition of HCl, R_{HCl}, in the range $1x10^{13}$ to $5x10^{13}$ molecule s^{-1} for the 0.78 cm^2 surface area of the Si-window leads to the formation of a crystalline HCl hydrate, $HCl•xH_2O$, whereas values outside of this range seemed to favor the formation of an amorphous HCl/H_2O mixture (Delval et al., 2003). The exact nature of this undoubtedly crystalline solid is still unknown. However, IR spectroscopic work on hydroxonium salts of the type $H_3O^+X^-$ suggests that the ν_1 and ν_3 peak positions of the symmetric and antisymmetric O-H stretch vibrations must correspond to a molecular structure in which the distance between the cation and anion is unusually large (Desbat and Huong, 1975; Iannarelli and Rossi, 2016). Recent work has shown that the presence of HCl hexahydrate ($HCl•6H_2O$) under the present experimental conditions could be safely excluded, however, the FTIR absorption spectrum clearly shows the presence of dissociated HCl within

412 the ice film (Iannarelli and Rossi, 2014). Akin to $HCl•6H_2O$ that is known to nucleate with
413 difficulty, crystallization of this unknown HCl hydrate seems to occur only under specific
414 conditions of temperature and/or HCl deposition. Owing to the quantitative control of HCl
415 deposition on the ice film in this work we infer the presence of at least two forms of HCl
416 hydrates in the temperature range chosen in analogy to previous work (Delval et al., 2003).
417 We clearly point out that the present work has been performed without simultaneous
418 spectroscopic control of the HCl/ice deposit that would have allowed the identification and/or
419 quantification of the molecular composition of the condensate. Because we lack a
420 spectroscopic probe for the ice film deposited on the QCMB in the present work we are
421 seeking a correlation between the type of HCl/H_2O deposit, either crystalline or amorphous,
422 and the relevant HCl deposition parameters. Previous work has revealed a distinctly different
423 temporal dependence of $J_{ev}(H_2O)$ between the crystalline and amorphous HCl hydrates with
424 the extent of H_2O evaporation from the film, both at low (Delval et al., 2003) and high
425 temporal resolution (Iannarelli and Rossi, 2014).
426 Datasets A and B have been characterized above in terms of a difference in the temporal
427 dependence of $J_{ev}(H_2O)$ as a function of increasing χ_{HCl} owing to H_2O evaporation. Taking
428 one example of each set Figure 2 reveals a distinct difference between experiment 7 (set B)
429 and 11 (set A) performed at T = 195 and 192 K, respectively, despite comparable HCl
430 deposition parameters (Table 2). At $t > t_D$ $J_{ev}(H_2O)$ for experiment 7 decreases at once with
431 χ_{HCl} in contrast to experiment 11 whose $J_{ev}(H_2O)$ value gradually starts to decrease at roughly
432 the same value of χ_{HCl} as experiment 7. In addition, in both cases the extent of the decrease of
433 $J_{ev}(H_2O)$ is roughly equal between t_D and t_{Hb} within less than a factor of two. Set B data are in
434 marked contrast to set A independent of the magnitude of χ_{HCl} which is highlighted by a
435 comparison of experiment 11 (set A) and 4 (set B) at 192 and 190 K, respectively. The abrupt
436 decrease of $J_{ev}(H_2O)$ for set B as well as the gradual decline for set A both at t_D occur before
437 HCl starts to evaporate from the sample at t_{Hb} and appear therefore to be independent of χ_{HCl}
438 within the range explored in the present work.
439 If we consider the mean value $<d_D>$ for data set B (Figures 4 and A2) we find 549.0 ±
440 120.0 nm compared to the 1'500 nm or so original ice thickness which corresponds to
441 approximately $8.5x10^{17}$ molecules of H_2O spread out over 0.50 cm^2. These H_2O molecules
442 are impacted by the presence of HCl to some extent because $J_{ev}(H_2O)$ is slowed down
443 significantly compared to pure ice. Previous results (Delval et al., 2003) on the deposition of
444 HCl on ice under conditions where the presence of an as yet unidentified crystalline hydrate
445 $HCl•xH_2O$ was confirmed by FTIR absorption led to the conclusion that on average the

amount of "trapped" H_2O within d_D corresponded to $1.2x10^{18}$ molecules starting with an original 1 μm thick ice film that was subsequently doped with HCl. This quantity of H_2O, when scaled from the 0.78 cm^2 area of the Si-window used for FTIR absorption to the area of 0.5 cm^2 of the QCMB leads to $7.7x10^{17}$ H_2O that is in satisfactory agreement with the present measurement of d_D or $8.5x10^{17}$ H_2O in the present work. We may add that the previous value of $1.2x10^{18}$ H_2O from the work of Delval et al. (2003) corresponding to d_D obtained in that work has been derived using HeNe interferometry which is a crude method for measuring the film thickness.

Specifically, considering the low value of d_D of experiments 1 and 10 (Table 2, Figure 4) we may define the behaviour of these condensates as "ice-like" because roughly 80% of the ice sample of roughly 1.5 μm thickness has evaporated at $J_{ev}(H_2O)$ of pure H_2O ice before it slows down. This decrease of $J_{ev}(H_2O)$ is a kinetic effect and acts on both the rate of evaporation as well as on the mass accommodation coefficient, the ratio of which remains constant because the characteristic vapor pressure of pure ice is maintained until $t = t_{He}$ when the sample runs out of H_2O and HCl. For sample 1 this conclusion is not too surprising owing to its extremely low HCl dose of 0.8 formal HCl monolayers. Sample 10 in comparison with the other members of data set A allows us to conclude that d_D is proportional to T_{ice} for data set A. Low temperatures prevent rapid diffusion of HCl into the bulk of the ice film which leaves the majority of the total mass of the thin film deposited void of any HCl. Therefore, a large fraction of the total mass of the thin film deposit evaporates at values of $J_{ev}(H_2O)$ characteristic of pure ice before it decreases to lower values when the presence of HCl slows down $J_{ev}(H_2O)$. Although our experiment does not reveal the location of the thin layer of HCl-contaminated ice, plausibility suggests that it is located on top of the ice film at the gas-condensed interface. The corollary of this is that it is impossible to "cap" a pure ice sample with a thin layer of an atmospheric condensable gas of lower vapor pressure in the hope to lower the vapour pressure of the condensate or slow down H_2O evaporation. This capping has been attempted many times, and examples abound. However, all attempts to lower the ice vapor pressure of the condensate using low amounts of polar contaminants of ice, such as HNO_3, HCl or HBr have proven futile to date (Biermann et al., 1998).

The other members of data set A are examples (experiments 2, 9, 11) with high values of d_D at higher temperatures and higher HCl doses (Table 2). Because of higher presumed interfacial HCl concentrations these samples experience a decrease in $J_{ev}(H_2O)$ owing to rapid diffusion of HCl into ice that affects the kinetics of evaporation to some depths of the ice film

corresponding to higher values of d_D. Both high HCl doses and high temperatures favor HCl contamination of deeper layers of the HCl film, hence high values of d_D.

Tentatively, we assign a crystalline, yet unknown molecular structure and stoichiometry to samples A in contrast to samples of dataset B that we identify with an amorphous structure in terms of a liquid HCl/H_2O mixture of variable composition. The main argument in favour of this assignment comes from recent kinetic work performed by Iannarelli and Rossi (2016a) who show that both $J_{ev}(H_2O)$ as well as the corresponding mass accommodation coefficient or the adsorption rate coefficient for H_2O adsorption is highly scattered for crystalline HCl hexahydrate whereas the amorphous mixture shows a significantly smaller scatter of the experimental and thermodynamic values (Iannarelli and Rossi, 2014). Figure A3 and A4 in the Appendix show this substantial difference in experimental scatter for the amorphous HCl/H_2O mixture (Figure A3) compared to crystalline HCl hexahydrate (Figure A4).

Figure 3 displays the range parameter $r^{b/e}$ as a function of R_{HCl} for all data displayed in Table 2. It is noteworthy that $r^{b/e}$ is in the range 20 to 27 for set B experiments 3, 4, 7 and 8 compared to set A data that seem to be scattered throughout the range. Members of data set B show a common average range for both d_D and $r^{b/e}$ which is the reason we tentatively assign these structures to amorphous liquid mixtures of high viscosity at the prevailing temperatures.

In conclusion, we take the simultaneous occurrence of the restricted range of the measured remaining thickness of ice d_D = 549.0 ± 120.0 nm together with a similarly restricted range of $r^{b/e}$ between 20 and 27 as well as the substantial overlap in R_{HCl} between the present and previous work (Delval et al., 2003) as an indication that set B evaporation experiments imply the presence of an amorphous HCl/H_2O mixture. In contrast, the scatter of the set A data across the range of $r^{b/e}$ and d_D values suggests the presence of an as yet unidentified crystalline HCl hydrate. If, and only if the HCl deposition conditions rapidly establish thermodynamic equilibrium, experiment 2 (low HCl flow rate) lies in the "ice" region in the temperature interval 192-210 K whereas experiment 11 (high HCl flow rate) should access crystalline HCl hexahydrate at 192 K but not at 210 K according to the revised HCl/H_2O phase diagram of Iannarelli and Rossi (2014). It remains to be seen whether or not the published FTIR absorption spectrum in Delval et al (2003) turns out to be identical to the expected crystalline HCl hexahydrate invoked as condensate in set A molecules, similar HCl deposition parameters notwithstanding. This proposal awaits further confirmation from FTIR spectroscopic work that will be combined in the future with the QCMB measurement. At this point we reiterate our earlier statement that T_{ice}, R_{HCl}, N^{dep}_{HCl} do apparently not control $J_{ev}(H_2O)$ of both datasets..

5. ATMOSPHERIC IMPLICATIONS

The evaporation range parameter $r^{b/e}$ may be used to quantitatively evaluate the upper limit of the evaporative lifetime extension of thin ice films under conditions of H_2O vapor subsaturation. In the interest of applying the data of the present work to atmospheric conditions we make the assumption that typical atmospheric Cirrus cloud particles of several μm diameter may be approximated by macroscopic thin films used to obtain the present data. The time t_{ev} in seconds to complete evaporation of an ice particle of radius r at a given relative humidity (rh) is given in equation 1 (Chiesa and Rossi, 2013; Iannarelli and Rossi, 2016a):

$$t_{ev} = \frac{(\frac{\rho N_L}{M})^{2/3}(\frac{r}{a})}{J_{ev}(1-rh)} \quad (1)$$

where ρ is the density of ice (0.916 and 0.925 g cm^{-3} at 273 and 173 K, respectively), M = 18 g mol^{-1} for H_2O, r and a are the ice particle radius and the distance between two molecular layers in H_2O(ice), respectively (Iannarelli and Rossi, 2016a). Equation 1 is based on a simple layer-by-layer evaporation model of H_2O(ice) from a spherical ice particle following a zero-order rate law for J_{ev} or a first order rate law for its inverse, namely H_2O adsorption or condensation. For a 10 μm diameter ice particle approximated by thin film experiment 1 (Table 2) at rh = 80%, T = 192 K, $J_{ev} = 3x10^{16}$ molecule s^{-1} cm^{-2} (Petrenko and Whitworth, 1999) and $a = 4x10^{-8}$ cm we obtain t_{ev} = 2050 s or 34 min. This is the value for a pure ice particle as $J_{ev}(H_2O)$ for pure ice has been used at the outset of the evaporation experiment and is a lower limit to the true evaporation time owing to the competition of mass transfer and heterogeneous chemistry (Seinfeld and Pandis, 1998). Using $r^{b/e}$ = 43 for experiment 1 t_{ev} is calculated to be 15 minutes and 24 hours for a 100 nm and 10 μm diameter particle, respectively, whereas the evaporative lifetime of an analogous pure ice particle would be only 21 s for the 100 nm diameter pure ice particle. Cirrus ice particles are frequently in the lower tens of μm size range resulting in a longer evaporation time considering that the simple evaporation model scales linearly with the radius of the ice particle. In conclusion we may state that, owing to the lifetime extension of ice particles contaminated by HCl, HNO_3 or other volatile atmospheric trace gases such as HOCl, HOBr or HONO, small particles may have a chance to survive subsaturated regions of the atmosphere so as to function as cloud condensation or ice nuclei for the following cloud cycle (Delval and Rossi, 2004; 2005; Pratte et al., 2006).

We would like to stress, that the variable $r^{b/e}$ factor displayed in Table 2 leads to a significant increase in the evaporative lifetime of a contaminated ice particle and amounts to a **kinetic effect** that does not affect the equilibrium vapor pressure of the ice particle in question: it is that of pure ice from the start of the evaporation experiment to $t = t_{He}$ and therefore affects both the rate of evaporation and accommodation equally. However, in cases the sample has lost most of its mass the vapor pressure decreases and becomes somewhat uncertain. In the present case the above statement is correct for $t = t_{Hb}$, that is before halogen evaporation. Of note is the fact, that the accommodation coefficient α is frequently less than unity, in contrast to what is often assumed, which will lower the rate of evaporation for pure ice, hence increase the evaporative lifetime of pure ice particles for $T \geq 180$ K as proposed in previous work (Delval and Rossi, 2004; 2005; Pratte et al., 2006).

As a token example of potential atmospheric importance of the measured evaporative lifetimes of ice particles laced with condensable atmospheric trace gases we may take the formation, persistence and evaporation of contrails and Cirrus clouds in the UT/LS. These are ice clouds forming on non-volatile ice nuclei at the corresponding temperature and relative humidity conditions and also frequently serve as reaction sites for heterogeneous atmospheric reactions in connection with ozone depletion and chlorine activation chemistry in the LS. Under certain conditions, Schumann and coworkers used the concept of the increase of the evaporative lifetimes of contaminated ice particles in aviation contrails occurring mostly in the UT, but sometimes also in the LS, in order to explain the persistence of ice clouds below ice saturation conditions up to a certain time duration. Ice clouds have a significant radiative forcing effect that is of interest in evaluating the climate forcing of high-flying aircraft in future aviation scenarios (Lewellen, 2014; Schumann et al, 2017; 2017a). However, the results of the present work show that the rate of evaporation of ice films doped with small amounts of acidic trace gases significantly slows down in a complex manner over the evaporation history of the film or particle, and that the application of equation (1) to atmospheric situations should be carried out with caution.

CONCLUSIONS

Despite the scatter of the values of $r^{b/e}$ and d_D in dataset A displayed in Figures 3 and 4 and the apparent lack of influence of the deposition parameters (T_{ice}, R_{HCl}, N^{dep}_{HCl}) on $J_{ev}(H_2O)$ we may state several key points from the present work:

(a) We observe two types of behaviour, both complex, as far as the temporal change of $J_{ev}(H_2O)$ with on-going evaporation of H_2O from a HCl/H_2O condensate is concerned. We have named it sets A and B that represent limiting behaviour as not all performed experiments fit into this scheme.

(b) At low temperature or low dose of deposited HCl (N^{dep}_{HCl}) set A samples, especially samples 1 and 10, reveal an "ice-like" behaviour that corresponds to a low value of d_D. This means that the HCl/H_2O condensate evaporates a large fraction of the sample thickness at a value of $J_{ev}(H_2O)$ characteristic of pure ice before slowing down at increasing mole fraction of HCl upon H_2O evaporation. This corresponds to a two-phase system consisting of a major ice-like and a minor HCl/H_2O phase having both significantly different values of $J_{ev}(H_2O)$.

(c) High values of d_D are observed at high T_{ice} or N^{dep}_{HCl} values for set A samples. This means that the sample evaporates H_2O at $J_{ev}(H_2O)$ characteristic of pure ice for a relatively short time of its evaporation history because the quantity of HCl is sufficient to decrease $J_{ev}(H_2O)$ already at high values of d_D by rapidly diffusing to deeper layers of the ice film. An equivalent way of expressing the point would be to state that d_D which is an indicator of the total mass of the ice film, is proportional to T_{ice} for Set A.

(d) Set A samples generally show scattered values of both d_D and $r^{b/e}$ values that we attribute to the existence of a two-phase binary system, namely a pure ice and a crystalline HCl hydrate phase of as yet unknown stoichiometry $HCl \bullet xH_2O$, but probably HCl Hexahydrate. At first the pure ice phase starts to evaporate as a whole for a fairly long time at characteristic values of $J_{ev}(H_2O)$ until the pure ice phase has disappeared, followed by the crystalline HCl/H_2O phase at a lower rate of $J_{ev}(H_2O)$ to attain the characteristic value for the evaporation of the crystalline $HCl \bullet xH_2O$ phase.

(e) Set B samples are tentatively identified as single phase binary amorphous mixtures of HCl/H_2O whose kinetic properties are uniform, thus fairly independent of the HCl concentration at the gas-condensed phase interface. The observation of a medium size average value for both $r^{b/e}$ and d_D is consistent with these observations and manifests itself as a continuous, yet gradual decrease of $J_{ev}(H_2O)$ with increasing χ_{HCl}. It is in distinct contrast to Set A where $J_{ev}(H_2O)$ values are those of pure ice until the ice phase has completely evaporated followed by a gradual decline of $J_{ev}(H_2O)$ when the crystalline HCl hydrate starts to decompose.

(f) It must be recalled that the vapour pressure of H_2O remained that of pure ice during most of the thickness of the H_2O/HCl condensate down to approximately 80 nm at which point we halted the evaporation experiment. This result is expected based on Raoult's law owing to the small average HCl mole fractions in doped ice used in the present work: It would make the decrease of the H_2O saturation vapour pressure unmeasurably small. The present results therefore primarily address the **kinetics** of H_2O evaporation which changes with the total mass of the thin film condensate and the concomitant increase in HCl concentration and/or mole fraction.

621 **References**

622

623 Abbatt, J. P. D. Interactions of atmospheric trace gases with ice surfaces: Adsorption and
624 reactions, Chem. Rev. **2003**, *103*, 4783-4800.

625 Banham, S. F.; Horn, A. B.; Koch, T. G.; Sodeau, J. R. Ionisation and solvation of
626 stratospherically relevant molecules on ice films, Faraday Discuss. **1995**, *100*, 321-
627 332.

628 Biermann, U.; Crowley, J. N.; Huthwelker, T.; Moortgat, G. K.; Crutzen, P. J.; Peter, T. FTIR
629 studies on lifetime prolongation of stratospheric ice particles due to NAT coating,
630 Geophys. Res. Lett. **1998**, *25*, 3939-3942.

631 Bolton, K.; Petterson, J. B. C. Ice-Catalyzed Ionization of Hydrochloric Acid, J. Amer. Chem.
632 Soc. **2001**, *123*, 7360-7363.

633 Bournel, F.; Mangeney, C.; Tronc, M.; Laffon, C.; Parent, P. Acidity of hydrogen chloride at
634 the surface of low-temperature 40–150 K water-ice films, Phys. Rev. B **2002**, *65*,
635 201404-1 to 201404-4.

636 Buch, V.; Dubrovskij, A., Mohamed, F.; Parinello, M.; J. Sadlej, J.; Hammerich, A.D.;
637 Devlin, J.P. Protonated Water HCl Hydrates as Model Systems for Protonated Water,
638 J. Phys. Chem. A 112, 2144-2161, 2008.

639 Buch, V.; Sadlej, J.; Aytemiz-Uras, N.; Devlin, J. P. Ice-Catalyzed Ionization of Hydrochloric
640 Acid J. Phys. Chem. A **2002**, *106*, 9374-9389.

641 Chiesa, S.; Rossi, M. J. $HCl{\bullet}6H_2O$ is metastable - IR spectroscopy, phase transitions and
642 kinetic/thermodynamic properties in the range 170-200 K, Atm. Chem. Phys. **2013**,
643 *13*, 11905-11923.

644 Chu, L. T.; Leu, M.-T.; Keyser, L. F. Uptake of HCI in Water Ice and Nitric Acid Ice Films,
645 J. Phys. Chem. **1993**, *97*, 7779-7785.

646 Delval, C.; Flückiger, B., Rossi, M. J. The Rate of Water Vapor Evaporation from Ice
647 Substrates in the presence of HCl and HBr: Implications for the Lifetime of
648 atmospheric Ice Particles, Atmos. Chem. Phys. **2003**, *3*, 1131-1145.

649 Delval, C.; Rossi, M. J. The kinetics of condensation and evaporation of H_2O from pure ice in
650 the range 173 to 223 K: A quartz crystal microbalance study, Phys. Chem. Chem.
651 Phys. **2004**, *6*, 4665-4676.

652 Delval, C.; Rossi, M. J. The influence of monolayer amounts of HNO_3 on the evaporation rate
653 of H_2O over ice at $179 \leq T/K \leq 208$: A quartz crystal microbalance study, J. Phys.
654 Chem. A **2005**, *109*, 7151-7165.

655 Delzeit, L.; Rowland, B.; Devlin, J. P. Infrared Spectra of HCl Complexed/Ionized in
656 Amorphous Hydrates and at Ice Surfaces in the 15-90 K Range, J. Phys. Chem. **1993**,
657 *97*, 10312-10318.
658 Delzeit, L.; Rowland, B.; Devlin, J. P. Ice Surface Reactions with Acids and Bases, J. Phys.
659 Chem. **1993a**, *97*, 10312-10318.
660 Delzeit, L.; Powell, K.; Uras, N.; Devlin, J. P. Ice Surface Reactions with Acids and Bases, J.
661 Phys. Chem. B **1997**, *101*, 2327-2332.
662 Desbat, B.; Huong, P. V. Spectres i.r. et Raman des sels d'hydroxonium $H_3O^+Cl^-$, $H_3O^+Br^-$ et
663 $H_3O^+SbCl_6^-$, Spectrochim. Acta, Part A **1975**, *31*, 1109-1114.
664 Devlin, J. P.; Uras, N.; Sadlej, J.; Buch, V. Discrete stages in the solvation and ionization of
665 hydrogen chloride adsorbed on ice particles, Nature **2002**, *414*, 269-271.
666 Devlin, J.P., Kang, H. Comment on «HCl adsorption on ice at low temperature: a combined
667 X-ray absorption, photoemission and infrared study» by P. Parent, J. Lasne, G.
668 Marcotte and C. Laffon, Phys. Chem. Chem. Phys. **2011**, 13, 7142, Phys. Chem.
669 Chem. Phys. **2012**, *14*, 1048-1049.
670 Donsig, H. A.; Vickerman, J. C. Dynamic and static secondary ion mass spectrometry studies
671 of the solvation of HCl by ice, J. Chem. Soc. Faraday Trans. **1997**, *93*, 2755-2761.
672 Ferriso, C. G.; Hornig, D. F. Infrared Spectra of Oxonium Halides and the Structure of the
673 Oxonium Ion, J. Chem. Phys. **1955**, *23*, 1464-1468.
674 Flückiger, B.; Thielmann, A.; Gutzwiller, L.; Rossi, M. J. Real-Time Kinetics and
675 Thermochemistry of the Uptake of HCl, HBr and HI on Water Ice in the Temperature
676 Range 190 to 210 K, Ber. Bunsenges. Phys. Chem. **1998**, *102*, 915-928.
677 Flückiger, B.; Delval, C. Unpublished observations on the behavior of dangling hydrogen
678 bonds (dH) in the presence of HCl at T < 120 K (2002). In essence, the dH absorption
679 intensity at 3396 cm^{-1} did not decrease in the presence of small HCl partial pressures
680 on the order of 3 x 10^{-6} Torr at ambient temperature or 4 ppb (Fig. 2.16, Christophe
681 Delval, PhD Thesis no. 3159, EPFL (2005))
682 Flückiger, B.; Rossi, M. J. Common Precursor-mediated Reaction Mechanism for the
683 Heterogeneous Interaction of D_2O, HCl, HBr and HOBr on Ice at low Temperatures, J.
684 Phys. Chem. A **2003**, *107*, 4103-4115.
685 Gertner, B. J.; Hynes, J. T. Molecular Dynamics Simulation of Hydrochloric Acid Ionization
686 at the Surface of Stratospheric Ice, Science **1996**, *271*, 1563-1566.

687 Gilbert, A. S.; Sheppard, N. Infra-red Spectra of the Hydrates of Hydrogen Chloride and
688 Hydrogen Bromide Absorption Bands of the $H_5O_2^+$ Species, J. Chem. Soc. Faraday
689 Trans. **1973**, *69*, 1628-1642.
690 Graedel, T. E.; Keene, W. C. Tropospheric budget of reactive chlorine, Global
691 Biogeochemical Cycles **1995**, *9*, 47-77.
692 Graham, J. D.; Roberts, J. T. Interaction of HCl with crystalline and amorphous ice:
693 implications for the mechanisms of ice-catalyzed reactions, Geophys. Res. Lett. **1995**,
694 *22*, 251-254.
695 Graham, J. D.; Roberts, J. T. Formation of HCl•6H_2O from ice and HCl under ultrahigh
696 vacuum, Chemom. Intell. Lab. Systems **1997**, *37*, 139-148.
697 Hanson, D.R. ; Ravishankara, A.R. Investigation of the Reactive and Nonreactive Processes
698 Involving $ClONO_2$ and HCl on Water and Nitric Acid Doped Ice, J. Phys. Chem.
699 **1992**, *96*, 2682-2691.
700 Houghton, J. T. et al.; eds., *Climate Change 2001: The Scientific Basis* (Cambridge Univ.
701 Press, New York 2001).
702 Hynes, R. G.; Mössinger, J.; Cox, R. A. The interaction of HCl with water-ice at tropospheric
703 temperatures, Geophys. Res. Lett. **2001**, *28*, 2827-2830.
704 Iannarelli, R.; Rossi, M. J. H_2O and HCl trace gas kinetics on crystalline and amorphous HCl
705 hydrates in the range 170 to 205 K: The HCl/H_2O Phase Diagram revisited, Atm.
706 Chem. Phys. **2014**, *14*, 5183-5202.
707 Iannarelli, R.; Rossi, M. J. The mid-IR absorption cross sections of α- and β-NAT
708 (HNO_3●$3H_2O$) in the range 170 to 185 K and of metastable NAD (HNO_3●$2H_2O$) in
709 the range 172-182 K, J. Geophys. Res. Atmos. **2016**, *120*, 11707-11727.
710 Iannarelli, R.; Rossi, M. J. Heterogeneous Kinetics of H_2O, HNO_3 and HCl on HNO_3 hydrates
711 (α-NAT, β-NAT, NAD) in the range 175-200 K, Atm. Chem. Phys. **2016a** *16*, 11937-
712 11960.
713 Jensen, E. J.; Toon, O. B.; Vay, S. A.; Ovarlez, J.; May, R.; Bui; T. P.; Twohy, C. H.;
714 Gandrud, B. W.; Pueschel, R. F., Schumann, U. Prevalence of ice-supersaturated
715 regions in the upper troposphere: Implications for optically thin ice cloud formation,
716 J. Geophys. Res. **2001**, *106*, 17253-17266.
717 Kang, H.; Shin, T. H.; Park, S. P.; Kim, I. K.; Han, S. J. Acidity of Hydrogen Chloride on Ice
718 J. Am. Chem. Soc. **2000**, *122*, 9842-9843.

719 Kong, X., Waldner, A., Orlando, F., Artiglia, L., Huthwelker, Th., Ammann, M., Bartels-
720 Rausch, Th. Coexistence of Physisorbed and Solvated HCl At Warm Ice Surfaces, J.
721 Phys. Chem. Lett. **2017**, *8*, 4757-4762.
722 Kuhs, W.F., Sippel, C., Falenty, F., Hansen, C.T. Extent and relevance of stacking disorder in
723 "ice I_c", PNAS (Proceedings of the National Academyof Science (USA)), **2012**, 109,
724 21259- 21264.
725 Leu, M.-T. ; Moore, S.B.; Keyser, L.F. Heterogeneous Reactions of Chlorine Nitrate and
726 Hydrogen Chloride on Type I Polar Stratospheric Clouds J. Phys. Chem. **1991**, *95*,
727 7763-7771.
728 Lewellen, D.C. Persistent Contrails and Contrail Cirrus. Part II: Full Lifetime Behavior, J.
729 Atmos. Sci. **2014**, *71*, 4420-4438.
730 Lu, Q. B. ; Sanche, L. Large enhancement in dissociative electron attachment to HCl
731 adsorbed on ice via transfer of presolvated electrons J. Chem. Phys. **2001**, *115*, 5711-
732 5713.
733 Lundgren, J. O.; Olovson, I. Hydrogen Bond Studies. XV. The Crystal Structure of Hydrogen
734 Chloride Dihydrate, Acta Cryst. **1967**, *23*, 966-970.
735 Lundgren, J. O.; Olovson, I. Hydrogen Bond Studies. XVI. The Crystal Structure of
736 Hydrogen Chloride Trihydrate, Acta Cryst. **1967a**, *23*, 971-976.
737 Marcy, T. P; Fahey, D. W.; Gao, R. S.; Popp, P. J.; Richard, E. C.; Thompson, T. L.;
738 Rosenlof, K. H.; Ray, E. A.; Salawitch, R. J.; Atherton, C. S.; Bergmann, D. J.;
739 Ridley, B. A.; Weinheimer, A. J.; Loewenstein, M.; Weinstock, E. M.; Mahoney, M. J.
740 Quantifying Stratospheric Ozone in the Upper Troposphere with *in situ* Measurements
741 of HCl, Science **2004**, *304*, 261-265.
742 Marti, J., Mauersberger, K. A survey and new measurements of ice vapor pressure at
743 temperatures between 170 and 250 K, Geophys. Res. Lett. **1993**, *20*, 363-366.
744 Mauersberger, K., Krankowsky, D. Vapor pressure above ice at temperatures below 170 K,
745 Geophys. Res. Lett. **2003**, *30*, 1121-1124.
746 Oppliger, R., Allanic, A., Rossi, M. J. Real-Time Kinetics of the Uptake of HOBr and
747 $BrONO_2$ on Ice and in the Presence of HCl in the Temperature Range 190 – 200 K, J.
748 Phys. Chem. A **1997**, *101*, 1903-1911.
749 Ortega, I. K.; Escribano, R.; Fernandez-Torre, D.; Herrero, V. J.; Maté, B.; Moreno, M. A.
750 The HCl hexahydrate: RAIR spectra and theoretical investigation, Chem. Phys. Lett.
751 **2004**, *396*, 335-340.

752 Parent, P., Laffon, C. Adsorption of HCl on the Water Ice Surface Studied by X-ray
753 Absorption Spectroscopy, J. Phys. Chem. B **2005**, *109*, 1547-1553.
754 Parent, P., Lasne, J., Marcotte, G., Laffon, C. HCl adsorption on ice at low temperature: a
755 combined X-ray absorption, photoemission and infrared study, Phys. Chem. Chem.
756 Phys. **2011**, *13*, 7142-7148.
757 Parent, P., Lasne, J., Marcotte, G., Laffon, C. Reply to the "Comment on "HCl adsorption on
758 ice at low temperature: a combined X-ray absorption, photoemission and infrared
759 study"" by J.P. Devlin and H. Kang, Phys. Chem. Chem. Phys. 2012, 14,
760 DOI:10.1039/c1cp22007a, Phys. Chem. Chem. Phys. **2012**, *14*, 1050-1053.
761 Petrenko, V. F., Whitworth, R. W. *The Physics of Ice*, Oxford University Press, **1999**.
762 Pratte, P.; van den Bergh, H.; Rossi, M. J. The kinetics of H_2O vapor condensation and
763 evaporation on different types of ice in the range 130-210 K, J. Phys. Chem. A **2006**,
764 *110*, 3042-3058.
765 Schriver-Mazzuoli, L., Schriver A., Hallou, A. IR-reflection-absorption spectra of thin water
766 ice films between 10 and 160 K at low pressure, J. Mol. Struct. **2000**, 554, 289-300.
767 Schumann, U.; Baumann, R.; Baumgardner, D.; Bedka, S.T.; Duda, D.P.; Freudenthaler, V.;
768 Gayet, J.-F.; Heymsfield, A.J.; Minnis, P.; Quante, M.; Raschke, E.; Schlager, H.;
769 Vazquez-Navarro, M.; Voigt, C.; Wang, Z. Properties of individual contrails: A
770 compilation of observations and some comparisons, Atm. Chem. Phys. **2017**, *17*, 403-
771 438.
772 Schumann, U.; Kiemle, C.; Schlager, H.; Weigel, R.; Borrmann, S.; D'Amato, F.; Krämer,
773 M.; Matthey, R.; Protat, A.; Voigt, C.; Volk, M. Long-lived contrails and convective
774 cirrus above the tropical tropopause, Atm. Chem. Phys. **2017a**, *17*, 2311-2346.
775 Seinfeld, J. H.; Pandis, S. N. *Atmospheric Chemistry and Physics, from Air Pollution to*
776 *Climate Change*, John Wiley and Sons, Inc. (**1998**).
777 Solomon, S.; Garcia, R. R.; Rowland, F. S.; Wuebbles, D. J. On the Depletion of Antarctic
778 Ozone, Nature **1986**, *321*, 755-758.
779 Solomon, S.; Borrmann, S.; Garcia, R. R.; Portmann, R.; Thomason, L.; Poole, L. R.; Winker,
780 D.; McCormick, M. P. Heterogeneous chlorine chemistry in the tropopause region, J.
781 Geophys. Res. (Atmos) **1997**, *102*, 21411-21429.
782 Taesler, I.; Lundgren, J. O. Hydrogen Bond Studies. CXXIX. An X-Ray Determination of the
783 Crystal Structure of Hydrogen Chloride Hexahydrate, $H_9O_4^+Cl^- \bullet 2H_2O$, Acta
784 Crystallogr. B **1978**, *34*, 2424-2428.

Tolbert, M. A.; Rossi, M. J.; Malhotra, R.; Golden, D. M. Reaction of Chlorine Nitrate with Hydrogen Chloride and Water at Antarctic Stratospheric Temperatures, Science **1987**, *238*, 1258-1260.

Uras, N.; Rahman, M.; Devlin, J. P. Covalent HCl at the Surface of Crystalline Ice at 125 K: The Stable Phase at Submonolayer Levels J. Phys. Chem. B **1998**, *102*, 9375-9377.

WMO (World Meteorological Organization) *Scientific Assessment of Ozone Depletion 2002*, Global Ozone Research and Monitoring Project, report no. 47, Geneva, **2003**.

Xueref, I.; Dominé, F. FTIR spectroscopic studies of the simultaneous condensation of HCl and H_2O at 190K – Atmospheric applications Atmos. Chem. Phys. **2003**, *3*, 1779-1789.

Yoon, Y. K.; Carpenter, G. B. The Crystal Structure of Hydrogen Chloride Monohydrate, Acta Cryst. **1959**, *12*, 17-20.

Zerefos, C. S.; Eleftheratos, K.; Balis, D. S.; Zanis, P.; Tselioudis, G.; Meleti, C. Evidence of impact of aviation on Cirrus cloud formation, Atmos. Chem. Phys. **2003**, *3*, 1633-1644.

The authors declare no competing interests regarding the present work.

Acknowledgement

We sincerely thank Dr. R. Iannarelli for Figures A3 and A4 displayed in the Appendix. We also would like to thank the Swiss National Science Foundation (SNSF) for unfailing support over the years. This work has been performed under SNSF grants no. 20-65299.01 and 200020-105471.

Table 1: Hardware parameters of both cryogenic sample supports

	Si Optical Window	QCM
Reactor temperature T_r [K]	320	
Reactor volume V_r [cm^{-3}]	2350	
Conversion factor (1/RT) Conv [molec cm^{-3} $Torr^{-1}$] with R=62398 [Torr cm^3 mol^{-1} K^{-1}]	$3.0 \cdot 10^{16}$ (1)	
Sample surface area [cm^2]	0.78	0.50
H_2O collision frequency with ice sample ω_{H2O} [s^{-1}]	5.08	3.26
H_2O effusion rate constant of calibrated leak $k_{esc}(H_2O)$ [s^{-1}]	0.064	
MS calibration factor for H_2O (m/z=18, Stirred Flow) C_{18}^{S-Flow} [molec s^{-1} A^{-1}]	$2.4 \cdot 10^{24}$	
MS calibration factor for H_2O (m/z=18, Dynamic) C_{18}^{dyn} [molec s^{-1} A^{-1}]	$1.7 \cdot 10^{25}$	
HCl collision frequency with ice sample ω_{HCl} [s^{-1}]	3.59	2.31
HCl effusion rate constant of calibrated leak k_{esc}(HCl) [s^{-1}]	0.047	
MS calibration factor for HC1 (m/z=36, Stirred Flow) C_{36}^{S-Flow} [molec s^{-1} A^{-1}]	$3.9 \cdot 10^{24}$	
MS calibration factor for HC1 (m/z=36, Dynamic) C_{36}^{dyn} [molec s^{-1} A^{-1}]	$6.3 \cdot 10^{24}$	
Calculated escape orifice area A_{esc} [mm^2]	1.0	

d = 10^4 Å or 1.0 µm for O.D.= 1.08 [A](2) at 3260 cm^{-1}	Calibration Factor	
	Temperature [K]	ratio(3)
	170	9.0
	180	8.0
	190	**7.8**
	193	6.0
	205	2.0
	208	1.9

[1] Wall temperature of the reactor at T = 320 K

[2] See (Delval et al., 2003)

[3] Corresponds to the ratio between the true number of molecules present on the QCM support and the number of molecules displayed by the IC5 controller (Delval et al., 2004)

Table 2 : Representative experimental results for the kinetics of H_2O evaporation in the presence of HCl for increasing HCl deposition temperatures at given rates of deposition R_{HCl} and doses of HCl N_{HCl}^{dep}. In the first column the number refers to the corresponding experiment and identifies the data displayed in Figure 2

Experiment number	T_{ice}	d_0	N^0_{H2O}	R_{HCl}	t_{dep}	N^{dep}_{HCl}	HCl	N^{evap}_{HCl}	χ^0_{HCl}	d_D	J^b_{ev}	J^e_{ev}	$r^{b/e}$
	[K]	[Å]	[molec]	[molec s^{-1}]	[s]	[molec]	ML	[molec]		[Å]	[molec cm^{-2} s^{-1}]	[molec cm^{-2} s^{-1}]	
10	174	15230	$2.4\cdot10^{18}$	$6.4\cdot10^{12}$	94	$6.0\cdot10^{14}$	4.8	$4.7\cdot10^{14}$	$2.5\cdot10^{-4}$	2733	$1.9\cdot10^{15}$	$4.4\cdot10^{14}$	4.3
5	188	13318	$2.0\cdot10^{18}$	$1.3\cdot10^{13}$	66	$8.7\cdot10^{14}$	7.0	$8.9\cdot10^{14}$	$4.4\cdot10^{-4}$	4540	$1.2\cdot10^{16}$	$3.9\cdot10^{15}$	3.1
4	190	14016	$2.1\cdot10^{18}$	$4.2\cdot10^{13}$	126	$5.4\cdot10^{15}$	43.2	$3.6\cdot10^{15}$	$2.6\cdot10^{-3}$	6360	$2.9\cdot10^{16}$	$1.4\cdot10^{15}$	20.7
6	190	13886	$2.1\cdot10^{18}$	$3.9\cdot10^{13}$	56	$2.2\cdot10^{15}$	17.6	$1.8\cdot10^{15}$	$1.0\cdot10^{-3}$	12861	$3.4\cdot10^{16}$	$1.7\cdot10^{16}$	2.0
1	192	14926	$2.3\cdot10^{18}$	$3.1\cdot10^{12}$	36	$1.0\cdot10^{14}$	0.8	$1.8\cdot10^{14}$	$4.3\cdot10^{-5}$	2823	$2.9\cdot10^{16}$	$7.1\cdot10^{14}$	40.8
2	192	14682	$2.3\cdot10^{18}$	$8.0\cdot10^{11}$	356	$2.6\cdot10^{14}$	2.1	$1.6\cdot10^{14}$	$1.1\cdot10^{-4}$	6817	$3.2\cdot10^{16}$	$6.5\cdot10^{14}$	49.2
11	192	14420	$2.2\cdot10^{18}$	$5.4\cdot10^{12}$	108	$5.4\cdot10^{14}$	4.3	$6.8\cdot10^{14}$	$2.4\cdot10^{-4}$	7717	$4.0\cdot10^{16}$	$7.9\cdot10^{14}$	50.6
3	193	14423	$2.2\cdot10^{18}$	$3.5\cdot10^{12}$	220	$7.0\cdot10^{14}$	5.6	$8.1\cdot10^{14}$	$3.2\cdot10^{-4}$	5659	$4.9\cdot10^{16}$	$1.8\cdot10^{15}$	27.2
7	195	12614	$1.9\cdot10^{18}$	$4.3\cdot10^{12}$	45	$1.9\cdot10^{14}$	1.5	$1.8\cdot10^{14}$	$1.0\cdot10^{-4}$	5325	$4.6\cdot10^{16}$	$2.0\cdot10^{15}$	23.0
8	205	13505	$2.1\cdot10^{18}$	$1.6\cdot10^{13}$	36	$5.9\cdot10^{14}$	4.7	$3.0\cdot10^{14}$	$2.8\cdot10^{-4}$	4607	$2.0\cdot10^{17}$	$1.0\cdot10^{16}$	20.0
9	210	13134	$2.0\cdot10^{18}$	$3.5\cdot10^{12}$	84	$3.0\cdot10^{14}$	2.4	$1.9\cdot10^{14}$	$1.5\cdot10^{-4}$	12136	$3.0\cdot10^{17}$	$1.8\cdot10^{16}$	16.7

Figure Captions

Figure 1: Typical experimental protocol of the evaporation at 192 K of an approximately 1.2 μm thick ice film doped with $5.4 \cdot 10^{14}$ molecules of HCl. This illustration corresponds to experiment 11 of Table 2. (○): ice thickness monitored by QCM (Å), (□): "apparent" H_2O evaporative flux, J^{QCM}_{ev} , monitored by QCM (molecule cm^{-2} s^{-1}), (+): I^{18} MS signal for H_2O, (×): I^{36} MS signal for HCl (A), (◊): J^{18}_{ev} evaporative flux calculated from I^{18} (molecule cm^{-2} s^{-1}), (Δ): Int(J^{18}_{ev}) time integral of J^{18}_{ev} (molecule cm^{-2}).

Figure 2: Change of the evaporative flux $J_{ev}(H_2O)$ as a function of the HCl mole fraction (χ_{HCl}) for the cases presented in Table 2 color-coded according to the corresponding experiment number in Table 2. The colored and circled numbers on axis "b" (left) correspond to $J_{ev}(H_2O)$ of pure ice before HCl deposition, the ones on axis "e" (right) are $J_{ev}(H_2O)$ at t = t_{He} at the end of HCl evaporation. The colored circles in the data field mark the value of $J_{ev}(H_2O)$ after HCl deposition at t = t_0 and are equal to $J_{ev}(H_2O)$ of pure ice. The start of any particular $J_{ev}(H_2O)$ curve as a continuous solid (bold) line occurs at t = t_D at 85% of $J_{ev}(H_2O)$ at t = 0 (pure ice value, colored circle or circled number on axis "b" to the left) and ends at t_{Hb}, the beginning of HCl evaporation as displayed in Figure 1B.

Figure 3: Synopsis of the dependence of the evaporation range parameter $r^{b/e}$ on the rate of deposition R_{HCl} of HCl for temperatures between 188 and 210 K. Each point is marked with the total number of HCl molecules (N_{HCl}) deposited on the ice film , the temperature of the ice film at HCl deposition and the experiment number (bold) referring to Table 2. The hashed area encompasses $r^{b/e}$ values for dataset B (experiments 3,4,7,8). The color code goes from low (blue) over medium (green) to high (red) temperatures.

Figure 4: Synopsis of the dependence of d_D on the rate of deposition R_{HCl} of HCl for temperatures between 188 and 210 K. Each point is marked with the total number of HCl molecules (N_{HCl}) deposited on the ice film, the temperature of the ice film at HCl deposition and the experiment number (bold font) referring to Table 2. The hashed area encompasses d_D values for dataset B (experiments 3,4,7,8). The color code goes from low (blue) over medium (green) to high (red) temperatures.

Figure 1

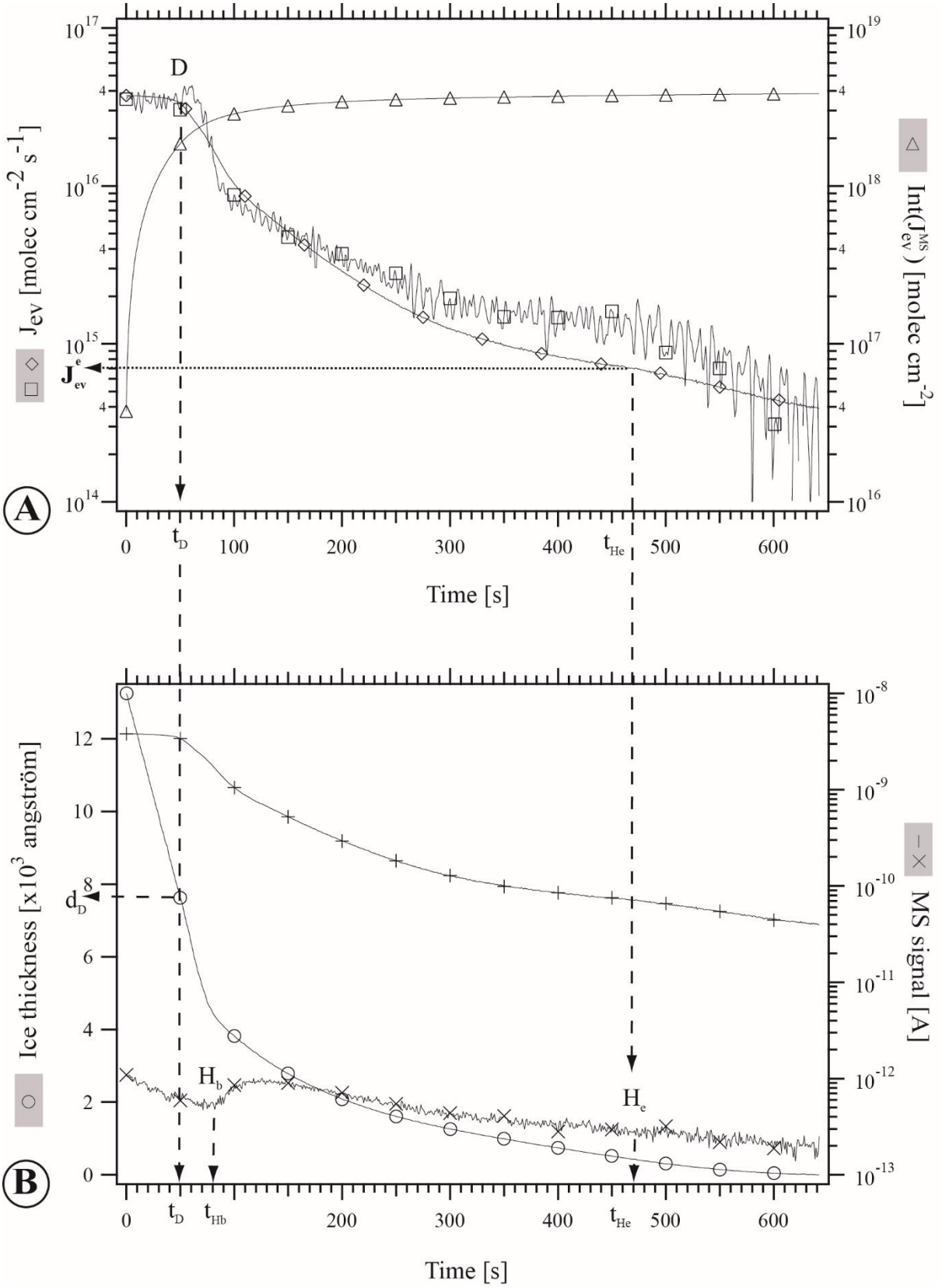
A
B
D
J_{ev} [molec cm^{-2} s^{-1}]
Int(J_{ev}^{MS}) [molec cm^{-2}]
J_{ev}^{e}
t_D
t_{He}
Time [s]
Ice thickness [x10^3 angström]
MS signal [A]
d_D
H_b
H_e
t_{Hb}

Figure 2

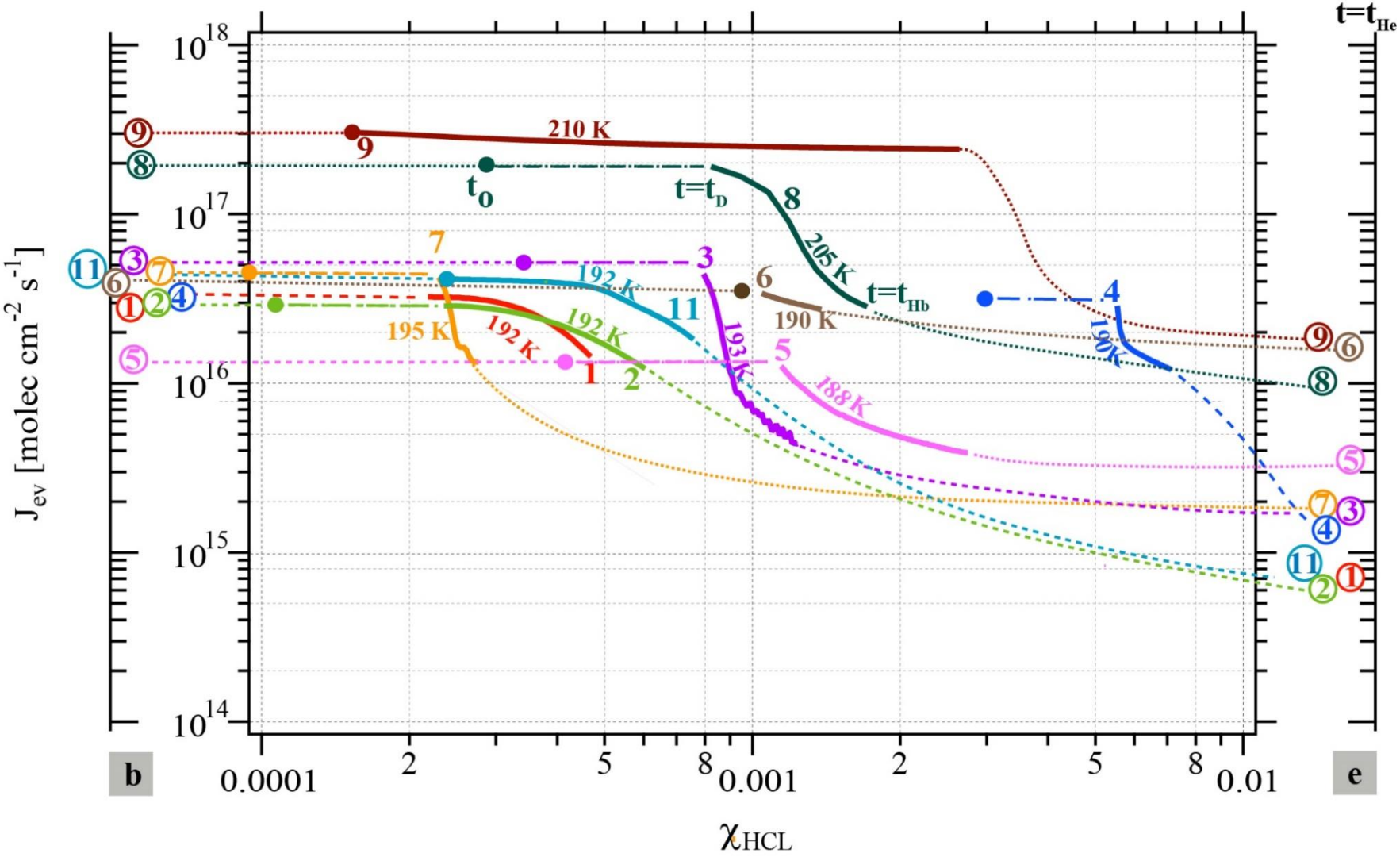
t=t_He
10^18
10^17
10^16
10^15
10^14
J_ev [molec cm^-2 s^-1]
210 K
t_o
t=t_D
205 K
t=t_Hb
192 K
195 K
192 K
192 K
190 K
190 K
193 K
188 K
b
e
0.0001
2
5
8
0.001
2
5
8
0.01
χ_HCL

Figure 3

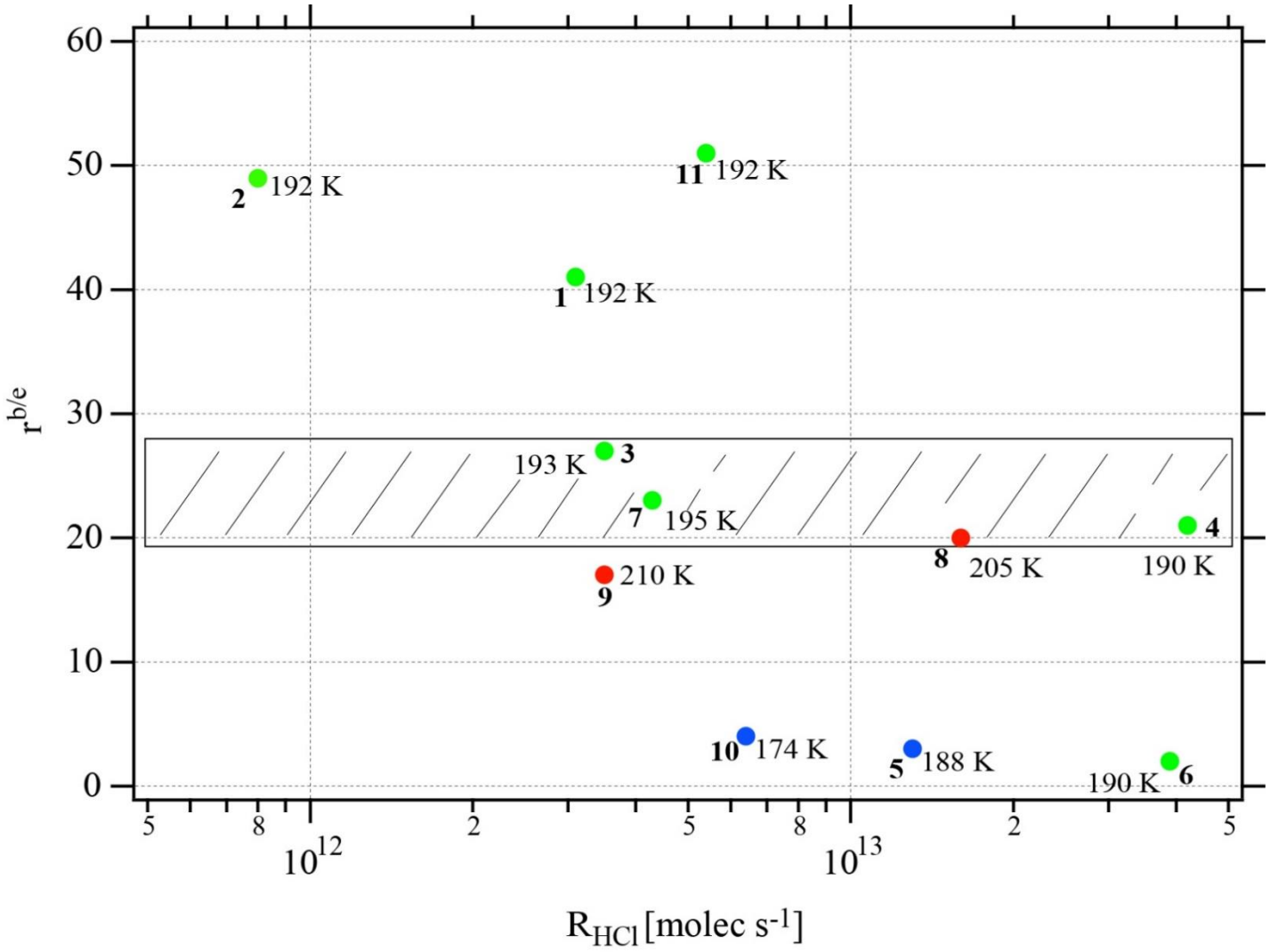
60
50
40
30
20
10
0
r b/e
2 192 K
11 192 K
1 192 K
193 K 3
7 195 K
4
8 205 K
190 K
9 210 K
10 174 K
5 188 K
190 K 6
5 8 2 5 8 2 5
10^12
10^13
R_HCl [molec s^-1]

Figure 4

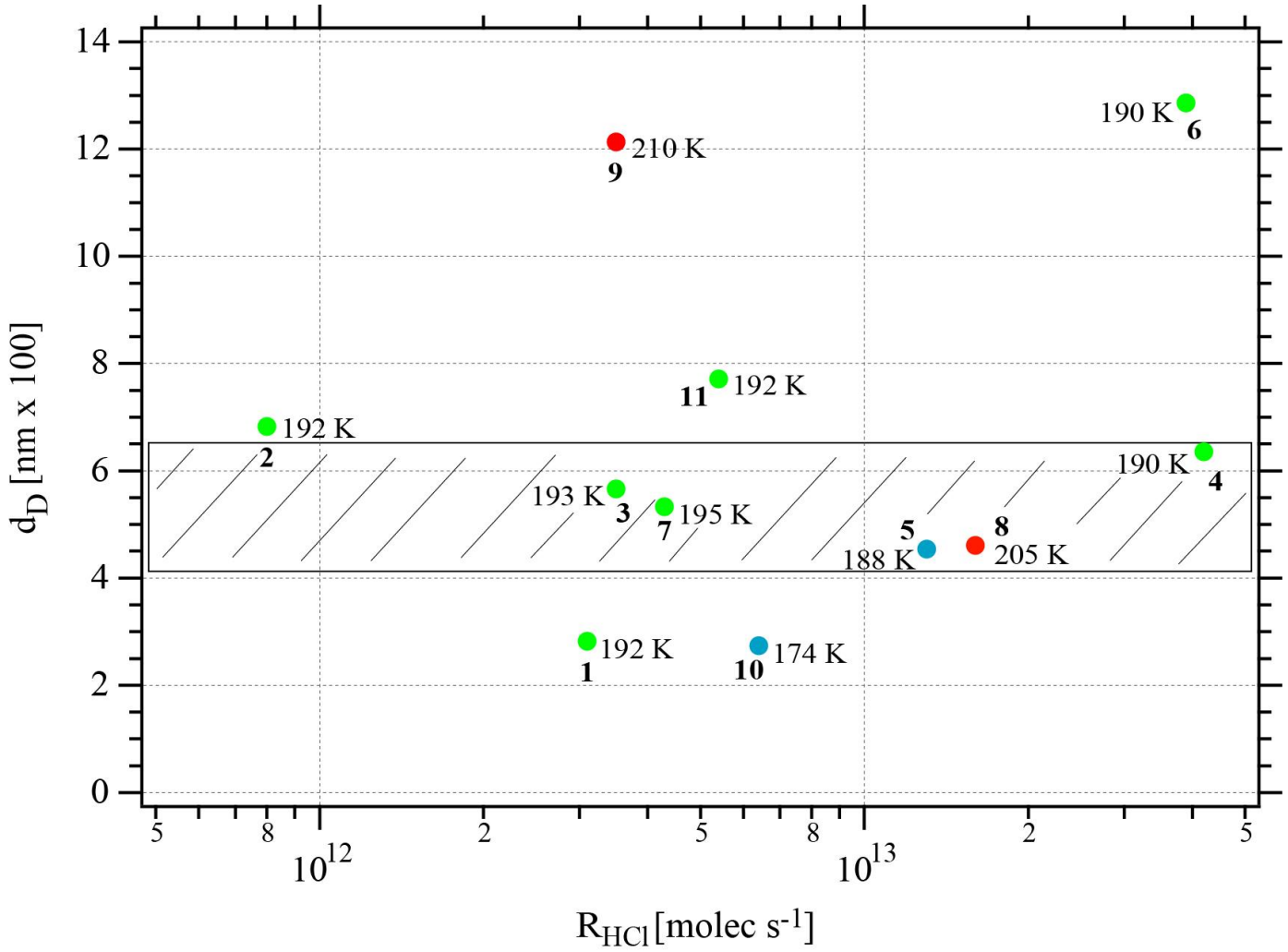
14
12
10
8
6
4
2
0
d_D [nm x 100]
5
8
10^{12}
2
5
8
10^{13}
2
5
R_{HCl} [molec s^{-1}]
192 K
2
210 K
9
190 K
6
192 K
11
193 K
3
195 K
7
190 K
4
188 K
5
205 K
8
192 K
1
174 K
10

APPENDIX A: Figures A1, A2, A3 and A4, Table A1

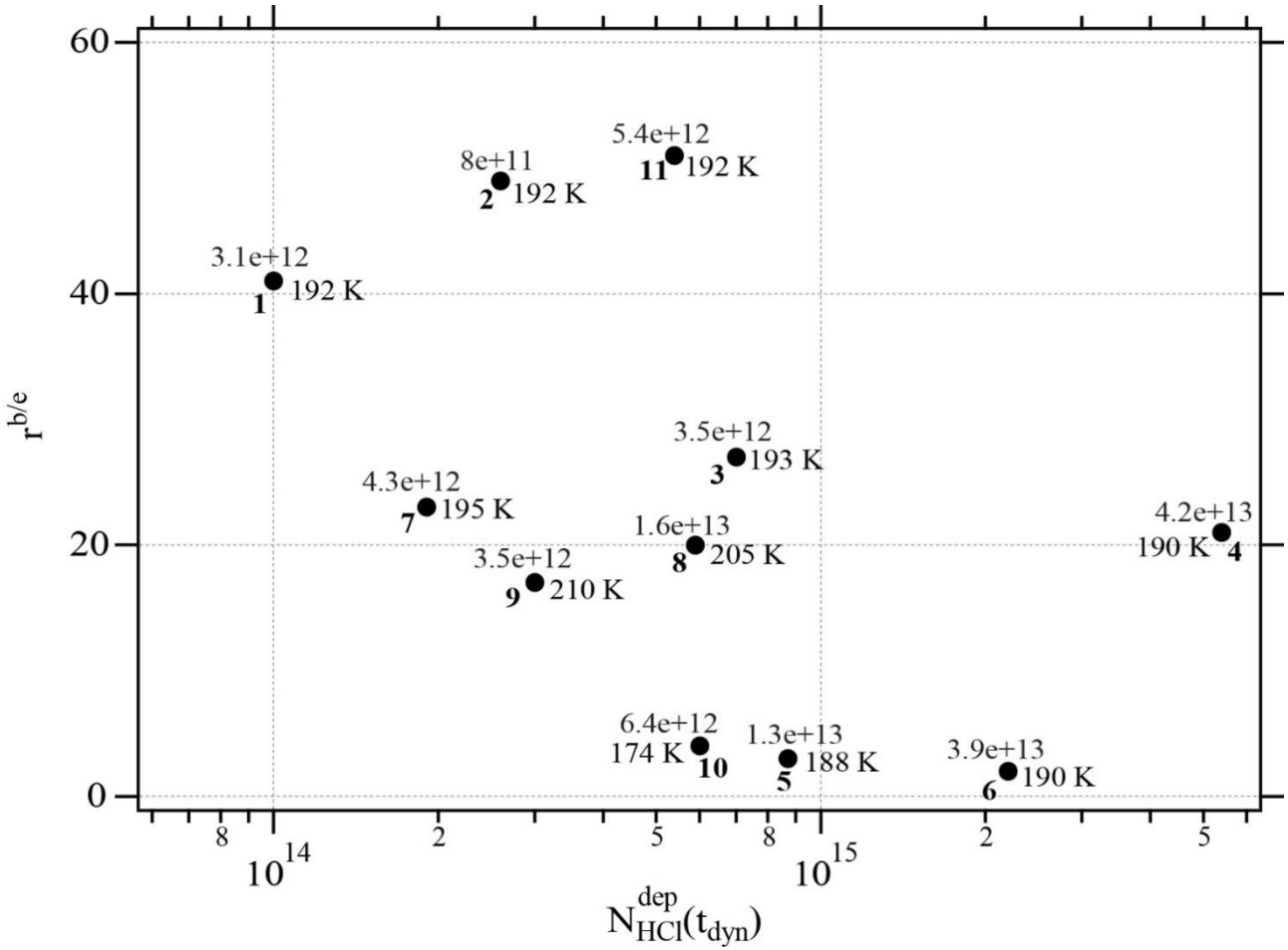

Figure A1: Synopsis of the dependence of the evaporation range parameter, $r^{b/e}$, on the number of adsorbed HCl, N_{HCl}^{dep}, adsorbed on ice for temperatures between 188 and 210 K. each point is marked with the deposition rate of HCl molecules in molec s^{-1} on the ice film, the temperature of the ice film and the experiment running number (bold) referring to Table 2.

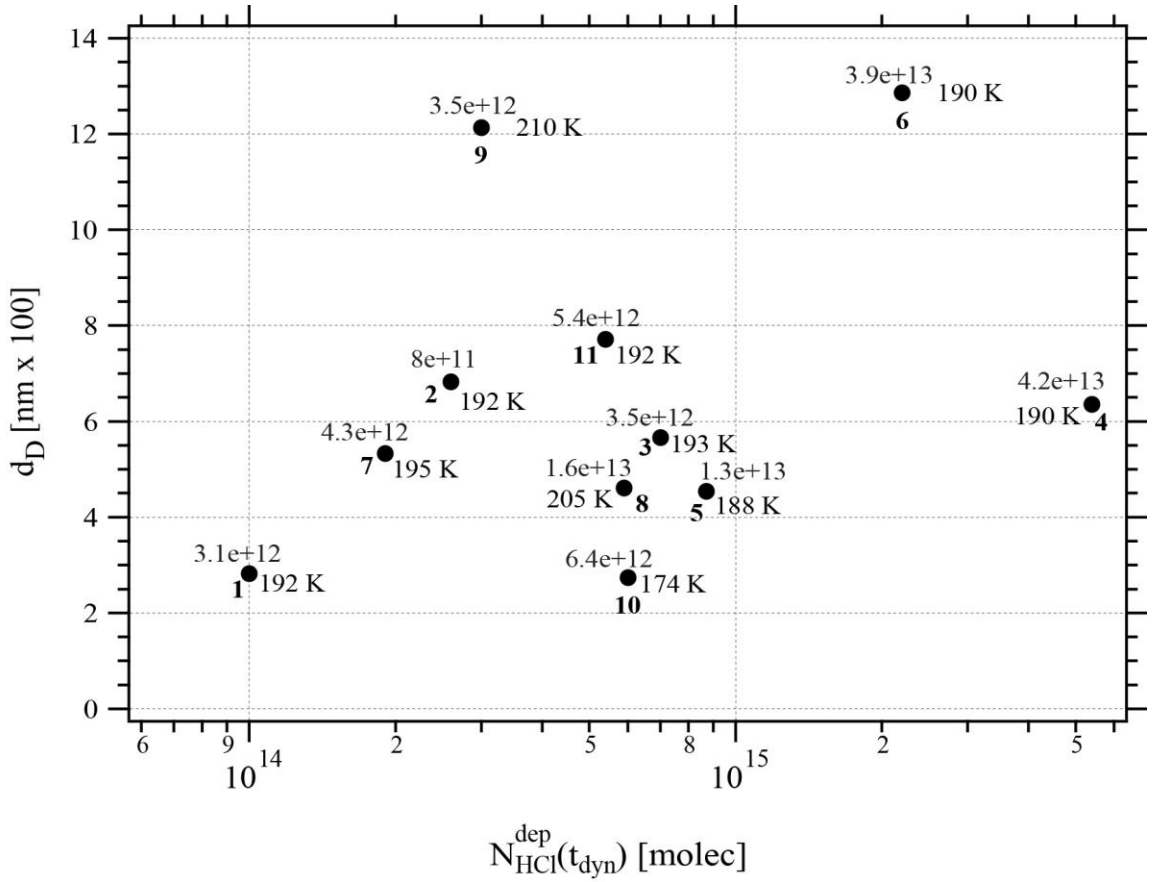

Figure A2: Synopsis of the dependence of the remaining thickness d_D on the number of adsorbed HCl, N_{HCl}^{dep}, dispensed on ice for temperatures between 188 and 210 K. Each point is marked with the deposition rate of HCl in molec s^{-1} on the ice film, the temperature of the ice film and the experiment running number (bold) referring to Table 2.

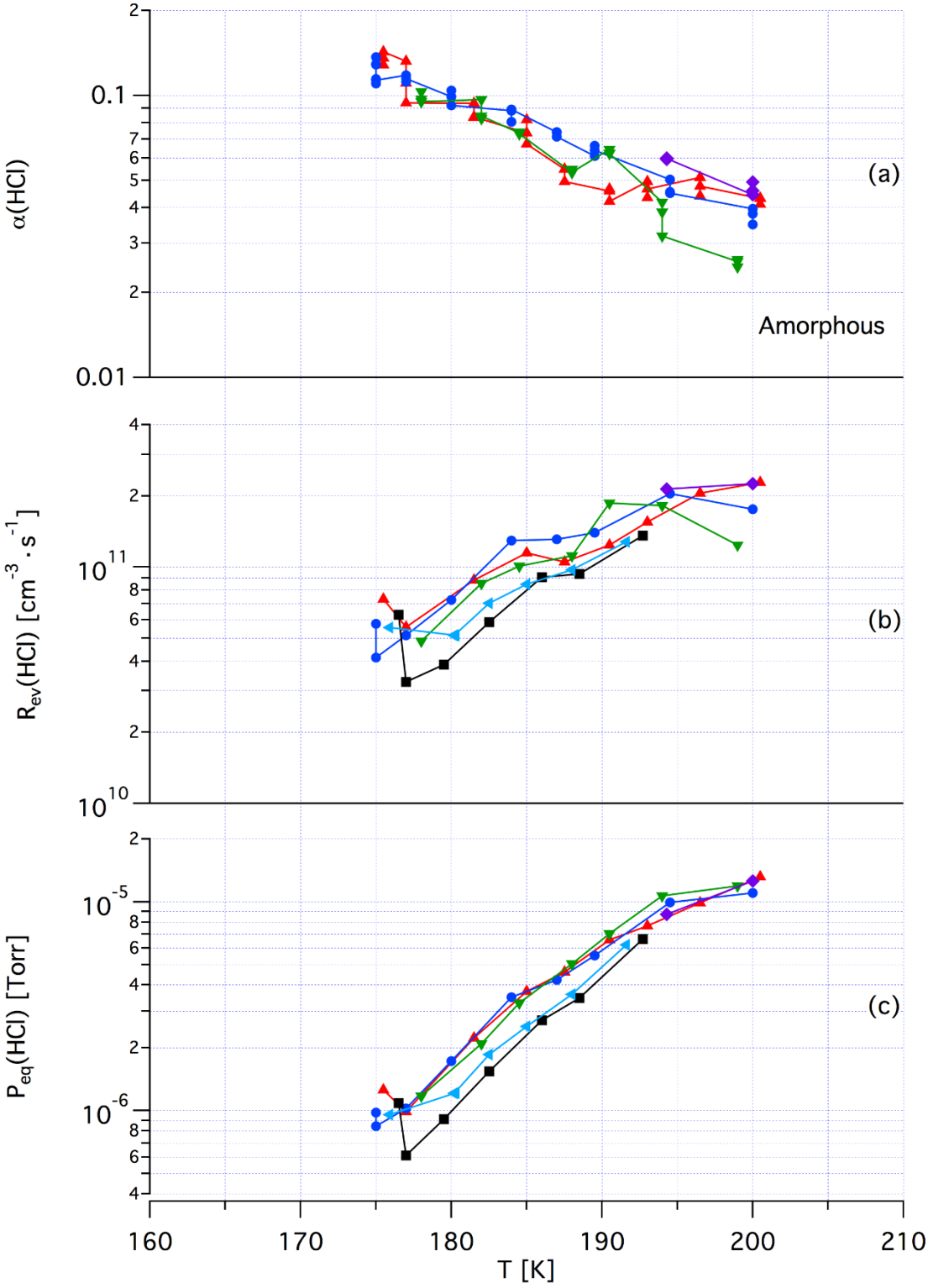

Figure A3: Synopsis of kinetic and thermodynamic results for an amorphous H_2O/HCl mixture using HCl as a probe gas. The symbols/colors used correspond to different experimental runs and the graphs show the scatter of the individual measurements within a series. Original data are published in Iannarelli, R. and Rossi, M.J. Atmos. Chem. Phys. 14, 5183–5204, 2014.

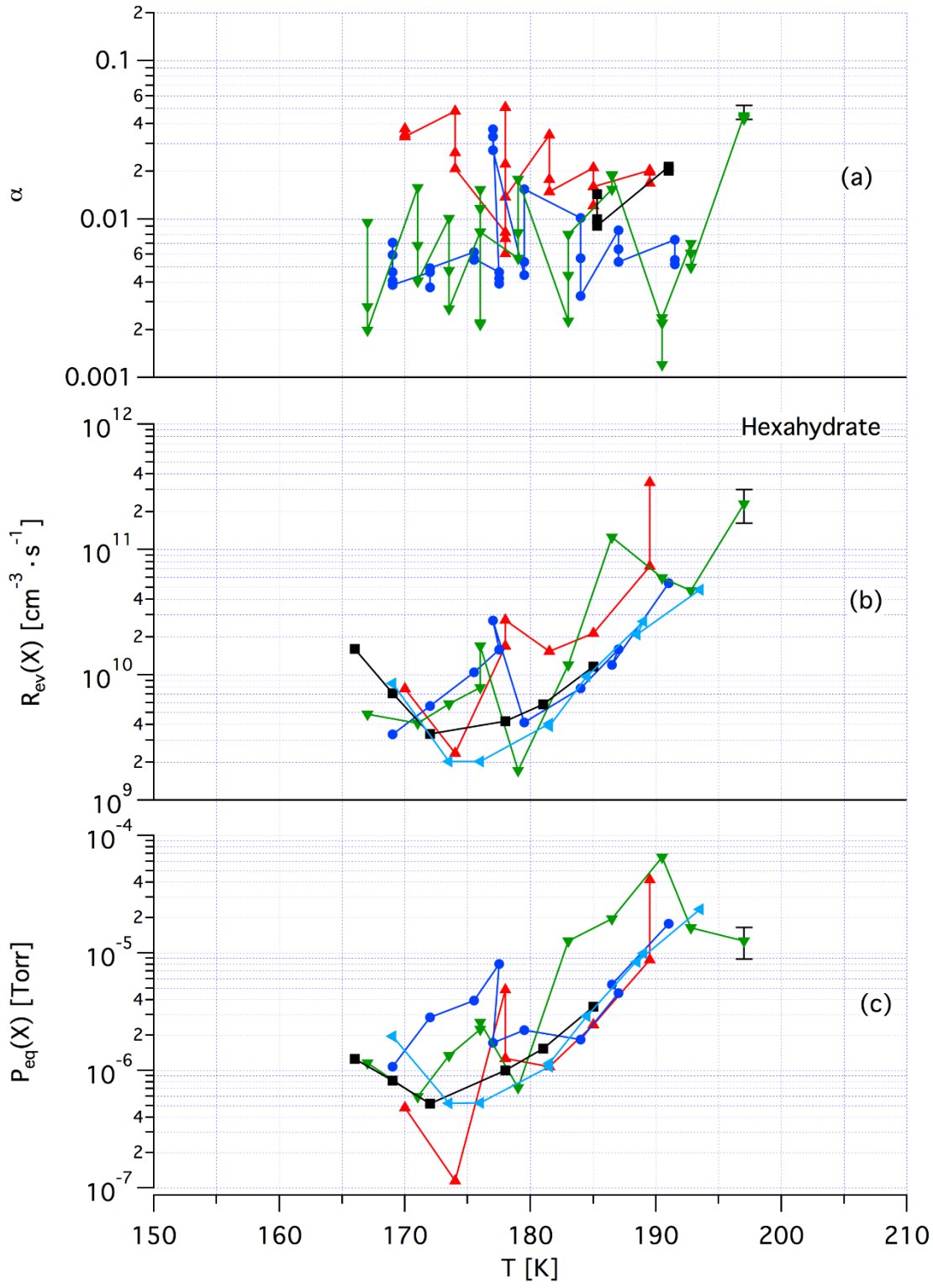

Figure A4: Synopsis of kinetic and thermodynamic results for crystalline HCl hexahydrate (HH) using X = HCl as a probe gas. The symbols/colors used correspond to different experimental runs and the graphs show the scatter of the individual measurements within a series. Original data are published in Iannarelli, R. and Rossi, M.J. Atmos. Chem. Phys. 14, 5183–5204, 2014.

Table A1: Brief Summary of the Amount of a Molecular Monolayer (Coverage) of HCl adsorbed on H_2O ice

Coverage / (molecule cm^{-2})	Temperature / K	Bibliographic Reference
$5.0\ 10^{15}$	200	Hanson, D. R., Mauersberger, K., HCl/H_2O Solid Phase Vapor Pressures and HCl Solubility in Ice, J. Phys. Chem., 94, 4700–4705, 1990
$1.0\ 10^{15}$	200	Abbatt, J.P.D., Beyer, K. D., Fucaloro, A. F., McMahon, J. R., Wooldridge, P. J., Zhang, R., Molina, M. J., Interaction of HCl vapor with water ice: implications for the stratosphere, J. Geophys. Res., 97, 15819–15826, 1992
$(2.0 – 3.0)\ 10^{14}$	191	Hanson, D., Ravishankara, A.R., Investigation of the Reactive and Nonreactive Processes Involving $ClON0_2$ and HCI on Water and Nitric Acid Doped Ice, J. Phys. Chem. 96, 2682-2691, 1992
$1.15\ 10^{15}$	183	Foster, K. L., Tolbert, M. A., George, S. M., Interaction of HCl with Ice: Investigation of the Predicted Trihydrate, Hexahydrate, and Monolayer Regimes, J. Phys. Chem. A, 101, 4979–4986, 1997
$2.5\ 10^{14}$	208	Interaction of HNO_3 with water-ice surface at temperatures of the free troposphere, Abbatt, J.P.D., Geophys Res. Lett. 24, 1479-1482, 1997
$3.1\ 10^{14}$	185	Flückiger, B., Thielmann, A., Gutzwiller, L., Rossi, M. J., Real time kinetics and thermochemistry of the uptake of HCl, HBr and HI on water ice in the temperature range 190 to 210 K, Ber. Bunsenges. Phys. Chem., 102, 915–928, 1998
$(1.1 \pm 0.6)\ 10^{14}$	201	Lee, S.-H., Leard, D. C., Zhang, R., Molina, L. T., Molina, M. J., The HCl + $ClONO_2$ reaction on various water ice surfaces, Chem. Phys. Lett. 315, 7–11, 1999
$(2.0 \pm 0.7)\ 10^{14}$	2001	Hynes, R. G., Mössinger, J. C., Cox, R. A.: The interaction of HCl with water-ice at tropospheric temperatures, Geophys. Res. Lett. 28, 2827–2830, 2001
$1.7\ 10^{14}$ $1.3\ 10^{14}$ $6.7\ 10^{13}$	190 200 210	Flückiger, B., Rossi, M.J., Common Precursor Mechanism for the Heterogeneous Reaction of D_2O, HCl, HBr, and HOBr with Water Ice in the Range 170-230 K: Mass Accommodation Coefficients on Ice, J. Phys. Chem. A 197, 4103-4115, 2003
2.3 to $2.7\ 10^{14}$	180 to 200	Henson, B. F., Wilson, K. R., Robinson, J. M., Noble, C. A., Casson, J. L., Worsnop, D. R.: Experimental isotherms of HCl and H_2O ice under stratospheric conditions, Connections between bulk and interfacial thermodynamics, J. Chem. Phys., 121, 8486– 8499, 2004